

Determination of Excitation Functions for $^{nat}\text{Br}(p,x)$ reactions
with Emphasis on the Production of the Radioisotope
Selenium-75.

Dawid de Villiers

Thesis presented for
the Degree of Master of Science in Physics
at the University of Stellenbosch



Supervisor: Prof W. A. Richter
Co-supervisor: Dr F. M. Nortier

Declaration:

I, the undersigned, declare that the work contained in this thesis is my own original work and has not previously in its entirety or in part been submitted at any university for a degree.

**Determination of excitation functions for $^{nat}\text{Br}(p,x)$ reactions with emphasis
on the production of the radioisotope Selenium-75**

Dawid de Villiers

Submitted to the Department of Physics
on 28 January 2000, in partial fulfillment of the
requirements for the degree of
Master of Science

Abstract

The radionuclide ^{75}Se ($T_{1/2} = 119.8$ days) decays to the stable isotope ^{75}As by 100 % electron capture. Applications of this radioisotope include its use as a radiotracer in agricultural investigations and as a potential irradiation source in high-activity brachytherapy. The application of this isotope as a radiotracer in clinical studies has been limited due to a lack of availability of carrier-free ^{75}Se .

In this study the excitation functions for the production of carrier-free ^{75}Se , other selenium radioisotopes and radiocontaminants produced via $^{nat}\text{Br}(p,x)$ nuclear reactions were measured by the use of the stacked foil technique.

Three separate stacks were assembled from aluminium and copper monitor foils and potassium bromide tablets. The latter were prepared by pressing KBr salt into tablets with a thickness of 200 mg/cm^2 and a diameter of 20 mm, which are sandwiched between thin Al foils. The monitor foils, with a diameter of 19 mm, were punched from foil sheets. The stacks were irradiated at proton beam energies of 100.9 MeV, 66.8 MeV and 40.4 MeV respectively at the National Accelerator Centre cyclotron facility.

After bombardment the KBr tablets were sealed in plastic bags to prevent the loss of any krypton isotopes produced. The gamma-ray spectra of the induced radioactivity in each of the target foils were recorded by means of a Ge-detector coupled with a SILENA 16-k multichannel analyser.

The measured excitation functions for the above-mentioned isotopes are presented. Where applicable the cross-section values are compared with previously published values, while the others are presented as new data. Theoretical calculations by means of the computer code ALICE (IPPE) were also done for comparison.

Bepaling van opwekkingskrommes vir $^{nat}\text{Br}(p,x)$ reaksies met die klem op die vervaardiging van die radioisotoop Selenium-75.

Dawid de Villiers

Voorgelê aan die Fisika Departement

op 28 Januarie 2000, vir gedeeltelike voldoening aan die

vereistes vir die graad van

Meester van die Wetenskap

Opsomming

Die radionuklid ^{75}Se ($T_{1/2} = 119.8$ dae) verval deur 100 % elektronvangs na die stabiele isotoop ^{75}As . Toepassings vir hierdie radioisotoop sluit in sy gebruik as 'n radiospoormiddel in landbou-ondersoeke en as 'n potensiële stralingsbron in hoë aktiwiteit bragiterapie. Die aanwending van hierdie isotoop as 'n radiospoorder in kliniese studies word egter beperk deur die gebrek aan beskikbaarheid van draer-vry ^{75}Se .

In hierdie studie is die opwekkingskrommes vir die produksie van draer-vry ^{75}Se , ander selenium radioisotope en radiokontaminante bepaal deur die $^{nat}\text{Br}(p,x)$ kernreaksies te meet met behulp van die foelie-stapel metode. Drie verskillende stapels, bestaande uit aluminium- en koper-monitor foelies en kalium-bromied tablette, is saamgestel. Laasgenoemde is voorberei deur KBr sout saam te pers tot tablette met 'n dikte van 200 mg/cm^2 en 'n deursnit van 20 mm en wat omsluit is met dun Al-foelies. Die monitor-foelies, met 'n deursnit van 19 mm, is gepons uit foelieplate. Die stapels is bestraal met protonbundels met energieë van onderskeidelik 100.9 MeV, 66.8 MeV en 40.4 MeV by die Nasionale Versneller Sentrum, Faure, se siklotron-fasiliteit. Na bombardering is die KBr tablette verseël in plastieksakkies om verliese van enige vervaardigde krypton isotope te verhoed. Die gamma-straal spektra van die geïnduseerde radioaktiwiteit in elke teiken is opgeneem met behulp van 'n Ge-detektor wat gekoppel was aan 'n SILENA 16-k multikanaal-analiseerder.

Bogenoemde isotope se gemete opwekkingskrommes word aangebied. Waar van toepassing word die kansvlakwaardes vergelyk met vorige gepubliseerde waardes terwyl ander aangebied word as die eerste data bekend. 'n Vergelyking met die teoreties berekende kansvlakwaardes van die rekenaar kode ALICE (IPPE) word ook gedoen.

ACKNOWLEDGEMENTS

I am greatly indebted to the following people for the role they played in making this thesis possible:

Dr. Meiring Nortier, co-supervisor, for his indispensable guidance and suggestions in the course of this investigation,

Prof. Werner Richter, supervisor, for the helpful discussions we had,

the National Accelerator Centre for the funding granted,

my brother, Frikkie for the technical drawings and other illustrations,

and my parents and friends for their support and encouragement.

Finally to my God, YAHWEH, all the glory, power and honour, for He has carried me every step of the way!

Opgedra aan my ouers, Paul en Maria de Villiers

CONTENTS

CHAPTER 1: MOTIVATION AND OUTLINE OF THIS THESIS	1
1.1 Introduction	1
1.2 The importance of nuclear data	1
1.3 The motivation for Selenium-75	2
1.4 The outline of the thesis	3
CHAPTER 2: THE PASSAGE OF ENERGETIC, CHARGED PARTICLES THROUGH MATTER	5
2.1 Introduction	5
2.2 Nature of charged particle interactions	5
2.2.1 Classification of heavy charged particle collisions	6
2.2.2 Energy loss and related effects of charged particles in their passage through matter	7
2.2.2.1 Stopping power	7
2.2.2.2 Path length and range	8
2.2.2.3 Energy and range straggling	9
2.2.2.4 Multiple scattering	9
2.2.3 Nuclear reactions	9
2.2.3.1 Reaction mechanisms	10
2.2.3.2 Q-value and threshold energy	10
2.2.3.3 Cross-sections	12
2.2.3.4 Excitation functions	13

CHAPTER 3: EXPERIMENTAL MEASUREMENT OF EXCITATION FUNCTIONS	15
3.1 Introduction	15
3.2 Experimental measurement of excitation functions	16
3.2.1 Stacked-foil technique	16
3.2.2 Stack preparation	16
3.2.3 Preparation of solid targets	16
3.2.3.1 Powder pressing techniques	17
3.2.3.2 Sandwiching of KBr targets	18
3.2.3.3 Preparation of monitor foils	19
3.2.4 Irradiations	19
3.2.5 Quantitative off-line gamma-ray spectroscopy	21
3.2.5.1 Counting procedure	21
3.2.5.2 Detector-and electronics setup	22
3.2.5.3 Energy calibration	22
3.2.5.4 Efficiency calibration	23
3.2.6 Data analysis	23
3.2.6.1 Procedures	23
3.2.6.2 Uncertainties	25
3.2.6.2.1 Experimental uncertainty in the cross-sections	25
3.2.6.2.2 Uncertainties in the energy values	25
3.2.6.2.3 Other sources of uncertainty	26
3.2.6.3 Proton flux measurements	26
3.2.6.3.1 Direct measurement	26
3.2.6.3.2 Monitor reactions	26
3.2.6.4 Energy and proton flux adjustments from the monitor reactions	27

CHAPTER 4: RESULTS AND DISCUSSION	32
4.1 Introduction	32
4.2 Selenium isotopes	32
4.2.1 Excitation functions	32
4.2.2 Routine production at the NAC	33
4.3 Comparison	35
4.3.1 Theoretical calculation of excitation functions	35
4.3.2 Published experimental excitation function data	35
CHAPTER 5: CONCLUSION	52
5.1 Conclusion	52
APPENDICES	54
A The calculation of the stopping power of a charged particle in the target material.	54
B Calculation of cross-section and production rates from stacked-foil data.	57
C Measured cross-sections for the radioisotopes produced in the monitor foils.	63
D Measured cross-sections for the radioisotopes produced in Br.	67
E Input parameters used in calculations with the computer code ALICE (IPPE)	71
BIBLIOGRAPHY	73

LIST OF FIGURES

2-1	Definition of the classical impact parameter	7
2-2	Stopping power as a function of energy	8
2-3	The different reaction mechanisms	14
3-1	The arrangement of foils inside the target holder	17
3-2	The punch and die set	18
3-3	The experimental setup	20
3-4	Block diagram of the electronic setup	22
3-5	Excitation function of ^{62}Zn before adjustments	29
3-6	Excitation function of ^{62}Zn after adjustments	29
3-7	Excitation function of ^{22}Na in the 66 MeV stack before adjustments	30
3-8	Excitation function of ^{22}Na in the 66 MeV stack after adjustments	30
3-9	Excitation function of ^{22}Na after adjustments	31
4-1	Excitation function of ^{75}Se	38
4-2	Comparison between the three selenium excitation functions	39
4-3	Thin target yield curves for the three selenium radioisotopes	40
4-4	Thick target yield curves for the three selenium radioisotopes	41
4-5	Excitation function of ^{72}Se	42
4-6	Excitation function of ^{73}Se	43
4-7	Excitation function of ^{75}Br	44
4-8	Excitation function of ^{77}Br	45
4-9	Excitation function of ^{80m}Br	46
4-10	Excitation function of ^{76}Kr	47
4-11	Excitation function of ^{77}Kr	48
4-12	Excitation function of ^{79}Kr	49
4-13	Excitation function of ^{71}As	50
4-14	Excitation function of ^{74}As	51

LIST OF TABLES

3-1	The duration of the different counting times	21
3-2	Isotopes identified for measurement and their decay data used	24
3-3	Summary of the experimental uncertainties	25
4-1	Thick target yield values of the selenium isotopes at different time periods	34
C-1	Measured cross-sections for the production of ^{62}Zn	63
C-2	Measured cross-sections for the production of ^{22}Na with 66 MeV protons	65
C-3	Summary of the measured cross-sections for the production of ^{22}Na	66
D-1	Measured cross-sections for the production of $^{74,71}\text{As}$	67
D-2	Measured cross-sections for the production of $^{80m,77,75}\text{Br}$	68
D-3	Measured cross-sections for the production of $^{79,77,76}\text{Kr}$	69
D-4	Measured cross-sections for the production of $^{75,73,72}\text{Se}$	70

Chapter 1

Motivation and Outline of this Thesis

1.1 Introduction

Today, radioisotopes are used extensively in the nuclear medicine field for diagnostic and therapy studies [Qai88], but their applications can also be found in industry [Nor90]. For the development of production procedures for these radionuclides, accurate measurements of the excitation functions are needed [Mil92].

In this study a production route for carrier-free ^{75}Se , by bombardment of natural bromine with protons, was explored in the energy range 16.1 - 100.9 MeV. Thorough measurements of the reaction excitation functions both for the investigated radionuclide and its by-products were made, aimed at determining the conditions for optimum production.

1.2 The importance of nuclear data

Although nuclear data are documented for several medical radioisotopes [Qai88], there is still a lack of data for the proton energy range of 40 - 100 MeV [Zai91]. Not only are new measurements needed, but an evaluation of the existing data are also highly desirable [Qai90]. The reason for such an evaluation is the great importance of accurate excitation function measurements

for the production of radionuclides in medical applications [Zai91], but also in other basic and applied physics fields [Bod93].

Nuclear data, including decay data and nuclear cross section data, are needed to fully utilise the application and production of radioisotopes [Qai82]. Decay data are needed to evaluate the suitability of a particular radioisotope for use in an application. Here accurate compilations do exist, for example [Reu83] and [Bro86]. Nuclear cross section data are important for the development of production procedures. They can be used to determine for which energy range the maximum yield of the desired radioisotope will occur while keeping the level of impurities as low as possible. This is especially important for production with proton beams in the intermediate energy range ($E_p > 20$ MeV) where a large number of competing reactions take place [Qai90]. The existence of the relevant excitation functions thus provides an easy way to determine the consequences of variations in the irradiation conditions of targets.

The aim of this study is therefore to obtain new data by exploring a new production route for ^{75}Se .

1.3 The motivation for ^{75}Se

The radionuclide ^{75}Se , with a half-life of 119.8 days [Reu83], decays to the stable isotope ^{75}As by 100 % electron capture. Its useful photon radiation includes gamma rays of 264.6 keV (59.1%), 136.0 keV (59.0%) and 279.5 keV (25.2%) [Reu83].

For a long time it was not used in medical applications due to the high radiation dose received by a patient [Mus89] and the lack of availability of carrier-free ^{75}Se limited its use in clinical studies [Ple90]. Nevertheless, it has since been used in pancreatic imaging [Hat72], labelling of viral proteins [Enz82] and selected as a potential irradiation source in high specific activity brachytherapy due to its longer half-life and lower energy gamma rays compared to ^{192}Ir [Wee86]. ^{75}Se has also been applied as a useful radiotracer in long-term environmental and agricultural investigations where the metabolism of natural selenium in soil-plant-animal systems was investigated [Dhi96]. The isotope is however, more useful for developing chemical

processing methods, particularly in the case of no-carrier added radioselenium and new routes of chemical synthesis [Eng90].

The production method commonly used for ^{75}Se involves the $^{74}\text{Se}(n,\gamma)^{75}\text{Se}$ reaction on highly enriched ^{74}Se in a nuclear reactor [Wee86]. Although batch yields are high the specific activity is low for this process. A more suitable method for accelerator production is the $^{75}\text{As}(p,n)^{75}\text{Se}$ process [Mus89], but it has the disadvantages of a limited energy range of 0 - 17 MeV [Ble94] and the product contains poisonous impurities [Fas98]. In this study an alternative and new production route via the $^{nat}\text{Br}(p,x)$ reactions is presented. The bromide target will make it easier to separate the ^{75}Se from the target material and the resulting impurities are not poisonous [Fas98]. The production can therefore easily and safely be incorporated into the existing radioisotope production programme of the National Accelerator Centre (NAC).

No data sets could be found in the literature for the complete ^{75}Se production route. Nevertheless, four data sets were available for the production of bromine and krypton radioisotopes via the $^{nat}\text{Br}(p,x)$ reactions: Diksic et al. [Dik79] for ^{75}Br , ^{77}Br , ^{80m}Br , ^{76}Kr , ^{77}Kr and ^{79}Kr , De Jongh, Brinkman and Linder [Dej79] for ^{75}Br , ^{76}Kr and ^{77}Kr , Colle and Kishore [Col74] for ^{79}Kr and Blosser and Handley [Blo55] for ^{79}Kr .

In addition to the above-mentioned experimental data, theoretical calculations by means of the computer code ALICE (IPPE) were also done for comparison.

1.4 The outline of the thesis

- In Chapter 2 the nature of charged particle interactions with matter and the observed physical phenomena relevant to radioisotope production and stacked-foil experiments are discussed. A brief overview of the three main reaction mechanisms is given, with emphasis on the proton as the incident charged particle.
- The experimental work done for the determination of the excitation functions is discussed in Chapter 3. This includes the techniques used in the target preparation, irradiations and data analysis. The detector and electronic setup, as well as the different uncertainties associated with the experiment are also given.

- The excitation functions for the production of ^{75}Se as well as other selenium isotopes and radiocontaminants were measured for protons incident on a KBr target. The measured cross section values together with the calculated thick and thin target yields for ^{75}Se are presented and discussed in Chapter 4. The values obtained in this study are compared with previously published data and theoretical calculations with the computer code ALICE (IPPE). The possibility of using this route for the production of ^{75}Se with the NAC's 66 MeV proton beam is also discussed.
- Chapter 5 summarizes the final conclusions on this study and some suggestions for further investigation are given.

Chapter 2

The Passage of Energetic, Charged Particles Through Matter

2.1 Introduction

At the NAC radioisotopes are produced by bombarding target material with energetic charged particles (e.g. 66 MeV protons). In the interaction between these charged particles and the target material, different physical processes, such as Coulomb interactions and nuclear reactions, take place. Some of these processes are discussed below.

2.2 Nature of the charged particle interactions

A fast charged particle such as a proton passing through matter interacts with atomic electrons and nuclei, but with different consequences for each type of interaction. Collisions with light atomic electrons can take up appreciable amounts of energy from the incident particle, without causing significant deflections, whereas in interactions with the massive atomic nuclei very little energy is absorbed, but scattering is much more prominent. In fact, the loss of energy by the incident particle is almost entirely due to collisions with atomic electrons, whereas its deflection is almost entirely due to scattering from atomic nuclei. Although these deflections are confined to rather small angles, so that the heavy incident particles keep a more or less straight-line path while losing energy, they still cause a beam of particles to broaden towards the end of their

range.

2.2.1 Classification of heavy charged particle collisions

As charged particles move through matter, three principle types of interactions between the incident particles and the material can be recognised:

- Collisions with the atoms of the material, where the atom as a whole participates in the collision. These interactions result in an excitation or ionisation of the atom and are called soft collisions.
- Hard collisions may occur when the interaction is between the incident particle and one of the atomic electrons. This process results in the ejection of an electron from the atom with considerable kinetic energy. This particle is called a delta ray.
- A charged particle having high kinetic energy, and which passes close to the atomic nucleus, may participate in a nuclear reaction. These interactions typically result in the emission of gamma rays and neutrons, although protons and alphas might also be ejected.

The values of the incident energy and the closest distance of approach (or impact parameter) determine which of the above-mentioned interaction types will dominate. (See Figure 2-1 for the definition of the impact parameter.) For a large impact parameter, soft collisions dominate, while hard collisions are more prominent when the impact parameter is less or equal to the radius of the atom. Nuclear interactions become more probable when the impact parameter becomes less than the radius of the nucleus.

Furthermore, if the incident energy is less than the Coulomb barrier presented by the target nucleus, only soft and hard collisions can take place. Nuclear reactions only become possible when the energy exceeds the Coulomb barrier.

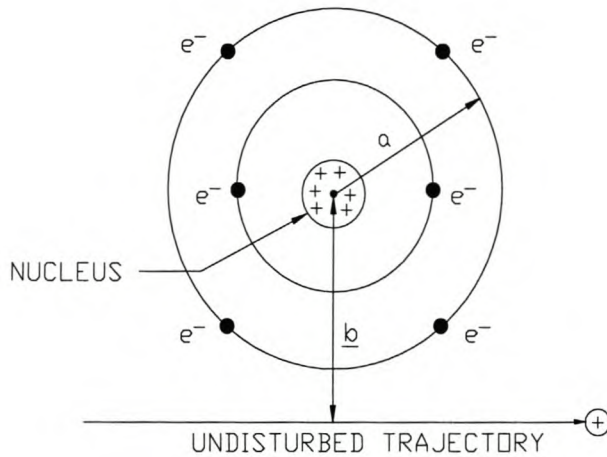


Figure 2-1: Two important parameters in charged-particle collisions with atoms: a is the classical atomic radius and b is the classical impact parameter.

2.2.2 Energy loss and related effects of charged particles in their passage through matter

2.2.2.1 Stopping power

As an incident particle traverses the target material, energy is lost due to the above-mentioned processes. The rate of energy loss per unit path length is called the stopping power ($S = -dE/dx$). The stopping power is used to calculate the particle's energy at a certain depth in the target material as well as the distance of penetration in the material.

In this study's non-relativistic energy range, the value for S is dominated by its dependence on the particle's velocity as $\frac{1}{v^2}$ (see Appendix A). This relation implies that the stopping power will increase as the charged particle velocity decreases along its path. The main reason for this is that more time is spent in the vicinity of the atomic electrons at low particle velocities and thus a larger energy transfer occurs. This relation is illustrated in Figure 2-2 where the stopping power is plotted as a function of incident energy.

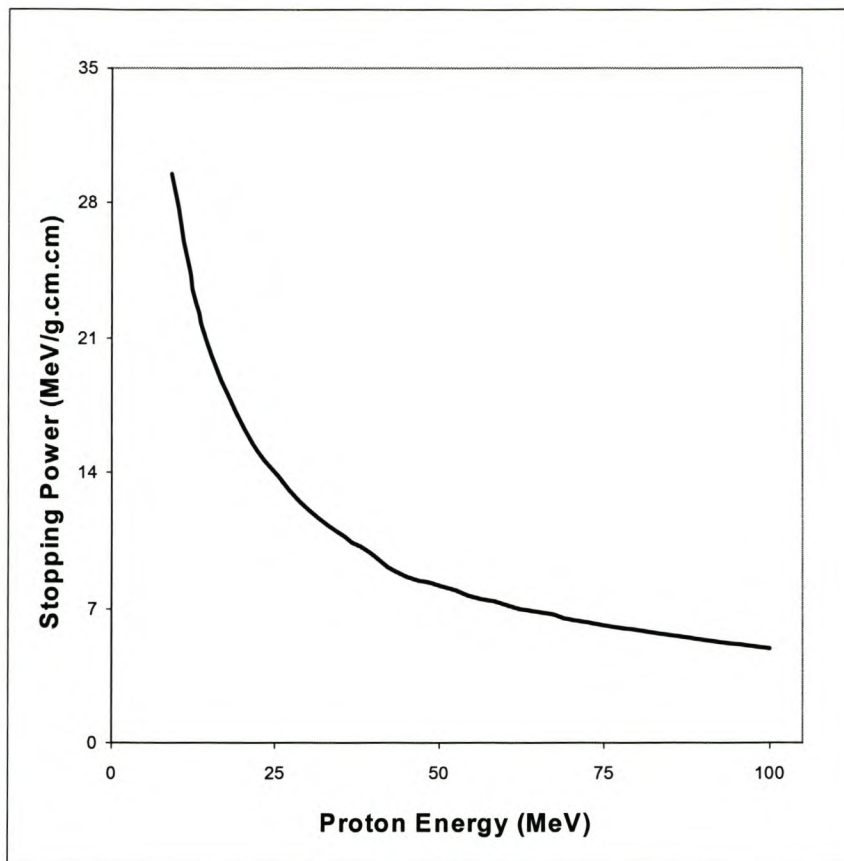


Figure 2-2: The calculated stopping power for protons in natural potassium bromide as a function of energy.

All stopping power values used in this study were calculated with the aid of the computer program STOPPING, which is based on the theory of Andersen and Ziegler [And77]. An overview of the formalism used is given in Appendix A.

2.2.2.2 Path length and range

The path length of a charged particle moving through matter is the total distance traversed by the particle whereas its range (or depth of penetration) is the sum of the projections of the individual path length increments along the incident direction of the charged particle. In the case of a fast charged particle, such as a 66 MeV proton, these two distances are nearly the same. Only at very low energies where single large-angle deflections during collisions become

more probable, can one expect significant differences between path length and range.

2.2.2.3 Energy and range straggling

The charged particles in a mono-energetic beam do not all lose exactly the same amount of energy while traversing a given thickness of material. The actual energy loss is a statistical phenomenon and, therefore, fluctuates around an average value as calculated from the stopping power. This fluctuation in energy is called the energy straggling and is seen as a spread in the energy distribution of the particles in the beam. The full-width-half-maximum (FWHM) of this energy distribution is a measure of the straggling and it increases with increasing depth of penetration, except near the end of the particle's path length where the energy distribution becomes distorted as a result of the reduction of the mean particle energy.

A process intimately related to energy straggling is that of range straggling. The fluctuation in the energy loss for a given penetration depth implies that the actual range of the individual particles should also fluctuate around an average value. This range straggling can be seen as a spread in the range values of the charged particles.

2.2.2.4 Multiple scattering

A charged particle traverses the target material in a random zigzag pattern due to a multitude of small-angle elastic Coulomb interactions with the atomic nuclei. For a beam of charged particles incident on a target this translates into a broadening of the beam with increasing depth in the target material.

2.2.3 Nuclear reactions

A nuclear reaction is an event where the incident particle interacts with the nucleus of one of the target material atoms. A comprehensive discussion of nuclear reactions is considered beyond the scope of this study, but the three main reaction mechanisms as well as related aspects will be briefly explained. Emphasis is placed on the proton as the charged particle since proton beams are routinely used for radioisotope production at the NAC.

2.2.3.1 Reaction mechanisms

As a proton moves through the target there exists a possibility of a non-elastic interaction with a target nucleus. In a close encounter with the nucleus it may produce internal disturbances in the nucleus and leave it in an excited state as a result of the inelastic nuclear scattering process. In an even closer encounter the proton can penetrate the target nucleus, causing a nuclear reaction.

At low energies the target nucleus captures the incident particle and a so-called compound nucleus is formed; during this phase the kinetic energy of the incident particle is shared among the nucleons until the incident particle is no longer distinguishable from the rest of the nucleons. After some time ($10^{-18} - 10^{-16}$ s) the probability for nucleon emission during statistical equilibrium becomes higher and nucleons are emitted until the nucleus energy is below the threshold for particle emission. Hereafter gamma rays are emitted until the nucleus is again in its ground state.

At much higher incident energies direct reactions occur. During the time the charged particle moves through the target nucleus (around 10^{-22} s) it may interact with one or more of the nucleons, transferring enough energy for them to be ejected from the target nucleus. This is called a direct reaction.

The last main reaction type is prominent at intermediate energies. In this pre-equilibrium process the incident particle penetrates the nucleus and it undergoes some nucleon interactions together with energy sharing, but particles will already be ejected long before statistical equilibrium is established.

2.2.3.2 Q-value and threshold energy

By using the initial and final mass energies in a nuclear reaction the Q value can be defined as [Kra88]:

$$Q = (m_{initial} - m_{final})c^2 \quad (2.1)$$

$$= (m_x + m_a - m_y - m_b)c^2, \quad (2.2)$$

where m_i is the mass according to the normal nuclear reaction notation of $x(a, b)y$.

This value may be positive, negative or zero. In the case of $Q > 0$, it is called an exothermic reaction and it implies that nuclear mass is released as kinetic energy of the products. On the other hand, during an endothermic reaction, with the Q value negative, the initial kinetic energy is converted to nuclear mass according to the special relativity relation $\Delta E = \Delta mc^2$. In this case there is also an absolute minimum kinetic energy below which a particular reaction is not energetically possible, and this value is called the threshold energy for that specific reaction. This value is defined as [Kra88]:

$$T_{th} = -Q \frac{m_y + m_b}{m_y + m_b - m_a}. \quad (2.3)$$

Another restriction on possible nuclear reactions is the repulsive Coulomb barrier. For a charged particle to enter the target nucleus it first has to overcome the repulsive Coulomb potential that exists between the nucleus and the positively charged particle. The height of this potential barrier V_c around a spherical nucleus of charge z_1e and radius of r_1 for a positive particle with charge z_2e and radius r_2 is classically predicted by placing the two particles in contact with each other and then by calculating V_c according to:

$$V_c = \frac{1}{4\pi\epsilon_0} \frac{z_1 z_2 e^2}{r_1 + r_2}. \quad (2.4)$$

If the quantum-mechanical viewpoint is taken, there exists a finite probability for a low energy proton to tunnel through this barrier, but the probability drops rapidly as the proton energy decreases.

The effective threshold is therefore the combination of the Q value and the Coulomb barrier. In the case of reactions with low Q values, such as (p, n) reactions this threshold is usually dominated by the height of the Coulomb barrier presented by the target nucleus, while in the case of higher energy reactions it is dominated by their Q -values.

2.2.3.3 Cross sections

A fundamental tool in the understanding of the interaction of a charged particle with nuclei is the concept of a reaction cross section. This is the relative probability for a specific nuclear reaction to occur at a particle energy E_i and is defined by [Kra88]

$$\sigma(E_i) = \frac{R}{I N}. \quad (2.5)$$

with R the number of nuclear reactions per unit time,

I the number of incident particles per unit time,

N the number of target nuclei per unit area.

Looking at the dimension, sigma can be seen as a hypothetical target area presented by the target nucleus, i.e. a reaction between the incident particle and the target nucleus will only occur if the incident particle passes through the hypothetical target area or cross section.

Radioisotopes can be produced via the decay of several short-lived precursors resulting from different reactions induced on a single isotope. As the production rate of each isotope in the chain is dependent on the formation of its precursor, the cross section value of the final product is usually the sum of all the precursors' individual cross sections. In this case the term cumulative cross section is used.

More often target material consists of a number of stable isotopes on which different types of reactions, leading to the formation of the same residual nucleus, can be induced. In this case it is not possible to distinguish each contribution to the final cross section and hence the term effective cross section is applicable. This cross section for the production of a particular radioisotope, at a specific incident energy; will be the sum of all the possible reaction cross sections contributing to its production, each weighted by the abundance of the target nucleus involved. In this study target material of natural isotopic composition was used and therefore the cross sections reported are actually effective cross sections, although hereafter not explicitly referred to as such.

The formulae used to calculate the sigma values in this thesis were taken from the program, SIGMA and incorporated into a *Microsoft Excel* spreadsheet. An overview of these formulae is given in Appendix B.

2.2.3.4 Excitation functions

The variation of the cross section for the formation of a particular residual nucleus with the bombarding particle energy is called the excitation function for the production of this residual nucleus. Excitation functions are commonly used to calculate production yields and radionuclidic impurity concentrations for a specific incident particle-energy window.

Both compound nucleus and pre-equilibrium reactions influence the shape of a particular radioisotope's excitation function. Usually the compound nucleus reaction cross section rises rapidly from the reaction threshold energy towards a peak and then falls due to the competition of other reaction channels producing other residuals. The tail region originates mainly from the contributions of pre-equilibrium processes. Direct reactions form the tip of the tail. Figure 2-3 shows an excitation function of an outgoing particle, indicating all three regions clearly. Excitation functions showing cross section as a function of the incident energy of the incoming particle, like those measured in this study, do not show these discrete contributions of the direct reactions..

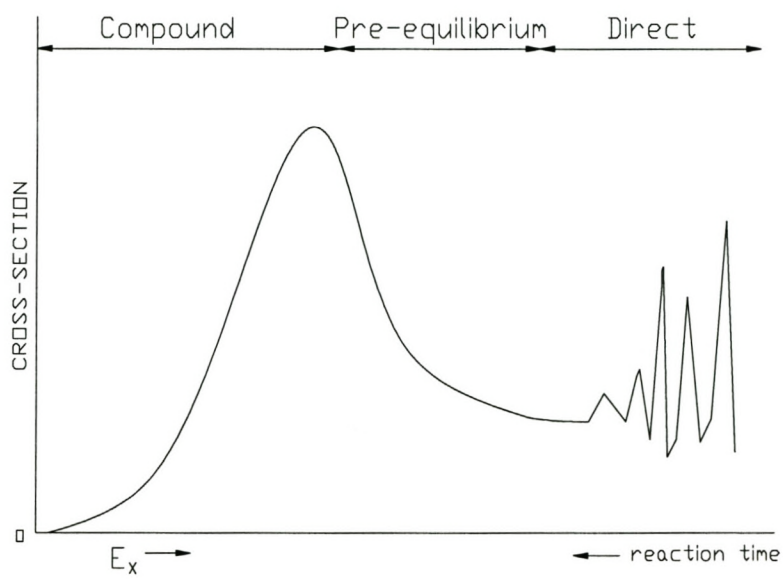


Figure 2-3: A typical energy spectrum of an outgoing particle showing the contributions of the different reaction mechanisms.

Chapter 3

Experimental Measurement of Excitation Functions

3.1 Introduction

A large number of data points is needed for the determination of an excitation function. In this work the cross sections for the production of ^{75}Se were measured by applying the stacked-foil technique using potassium bromide (KBr) as target material. This technique and the details of the preparation of the stacks are discussed, which include the pressing of the tablets and sandwiching. The preparation of monitor foils and their use as a method of measuring the proton flux are also presented.

The experiment started out with three separate irradiations that lasted for one hour each. By the use of off-line gamma-ray spectroscopy and the application of decay data the spectra were analysed and cross sections calculated. This process and the uncertainties associated with this calculation are explained. The detector and electronic setup are also described.

3.2 Experimental Measurement of Excitation Functions

3.2.1 Stacked-foil technique

In this technique a number of targets (salt tablets and metal foils) are combined in a stack and irradiated. Afterwards the activity in each target is measured and the spectra analysed by means of off-line gamma-ray spectroscopy. As the incident proton beam traverses the stack, energy is lost along the way so that a different energy is applicable at each foil in the stack. Thus a single irradiation allows one to measure several cross section data points at different proton energies. Uncertainties in the energy values due to straggling were minimized by dividing the 1.9 - 100.9 MeV range into three smaller regions with nominal primary incident energies of 40, 66 and 100 MeV. A separate stack of foils was prepared for each region. In the stacks energies ranged from 100.9 - 57 MeV, 67 - 24 MeV and 40 - 1.9 MeV.

3.2.2 Stack preparation

The stacks were assembled from three types of foils: KBr, Al and Cu foils. They were arranged in such a way that an Al and one or more Cu foils followed each of the KBr foils. A typical arrangement is schematically shown in Figure 3-1. The KBr foils with a diameter of 20 mm were sandwiched between two thin (0.020mm thick) Al foils with a diameter of 19 mm. The copper and aluminium disks also had a diameter of 19 mm. The thicknesses of the stacks were adequate to provide satisfactory energy overlaps of the three different data sets.

The KBr-foils served as the target foils for the measurement of proton-induced reactions on Br. Each of the target foils was followed by an Al monitor foil. Additional degradation of the beam energy within the stack was accomplished by means of Cu foils. For incident proton energies of less than 25 MeV the Al monitor foils were replaced by Cu monitor foils.

3.2.3 Preparation of solid targets

Targets were made from KBr salt powder pressed into tablets and sandwiched between two thin Al foils. Selenium-75 is commonly produced in a nuclear reactor by highly enriched ^{74}Se capturing thermal neutrons through the reaction: $^{74}\text{Se}(n,\gamma)^{75}\text{Se}$ [Wee86]. At proton energies

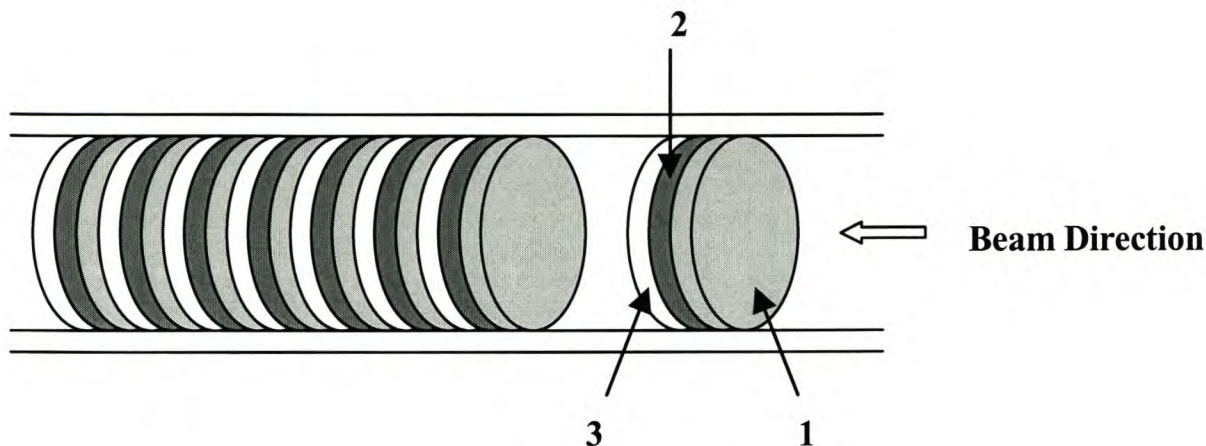


Figure 3-1: The arrangement of foils inside the target holder: KBr tablet (1), Al-foil (2) and Cu-foil (3).

below about 20 MeV the $^{75}\text{As}(p,n)^{75}\text{Se}$ process seems feasible [Ble94] for the production of carrier-free ^{75}Se at an accelerator. In this work, a new accelerator production method for higher energy protons, using potassium bromide targets utilising the reaction $^{nat}\text{Br}(p,x)$ is presented. Bromine as a target material has the advantages that the chemical separation of the ^{75}Se product is relatively easy and there is no risk of poisonous chemical impurities [Fas98].

3.2.3.1 Powder pressing technique

Potassium bromide salt powder and a punch and die set were used in the preparation of the salt tablets. The salt was obtained from SAARCHEM (South Africa) with a purity value of 99.5%. A 0.628 g amount of salt was used to press a tablet with a radius of 10 mm and a thickness of 200 mg/cm^2 . For the 40 MeV stack the tablets were made thinner by reducing the amount of salt to 0.314 g. This was done to still obtain twelve data points and to account for the steep slope in the low energy region, especially near the threshold, of an excitation function and the higher stopping power due to the proton's lower velocity (see § 2.2.2.1).

For each tablet the amount of salt was weighed out by hand and stored in small bottles. As KBr is hygroscopic the salt was dried under vacuum in a freeze drier, at a temperature of 223 K for at least 48 hours, before the pressing phase started.

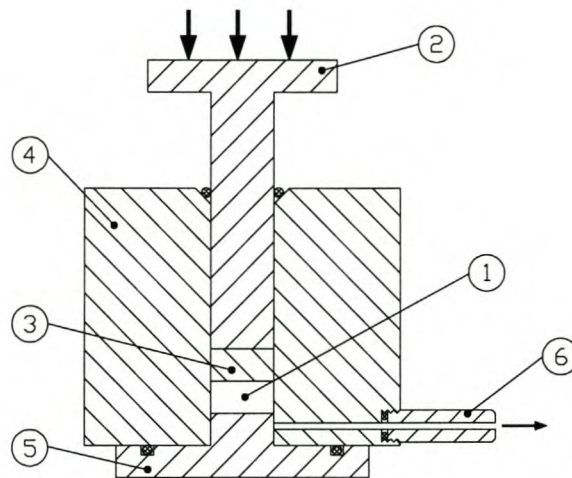


Figure 3-2: A drawing of a punch and die set used for pressing the KBr tablets, showing the KBr salt (1), the punch (2), insert (3), body (4), base (5) and connection for vacuum (6).

The pressing operation was done using a punch and die set (see Figure 3-2) in combination with a 300 ton hydraulic press which was operated at a pressure of $6.28 \text{ ton}\cdot\text{cm}^{-2}$ for 10 seconds. A thin Al-foil was placed in the punch shaft with the salt and another thin Al-foil on top. This combination was then pressed into a disc having a diameter of 20 mm. Twelve tablets were prepared in this way for each stack and stored under vacuum in a desiccator until about an hour before bombardment. This was done to avoid any moisture absorption that could influence the mass and therefore result in inaccurate cross section data and energy values. The tablet masses were determined again just before placement in the target holder.

3.2.3.2 Sandwiching of KBr targets

Gaseous isotopes escaping from the targets at any time before counting could result in erroneous cross section values. Krypton isotopes, among others, are produced by nuclear reactions in the KBr targets. Since krypton is a gas and since some of these krypton isotopes act as precursors in the formation of other isotopes, their loss resulting from their escape from the targets could lead to inaccurate cross section values. To prevent this, each of the targets was sandwiched

between two thin (0.00461g/cm^2 thick) aluminum foils during the pressing stage. The foils with a diameter of 19 mm were punched from a 15.3 cm x 14.8 cm sheet of aluminum foil. In another similar experiment [Dik79] significant losses of krypton were not observed when the same sandwiching technique was used.

3.2.3.3 Preparation of the monitor foils

Aluminium disks with a diameter of 19 mm and a thickness of 0.06786 g/cm^2 were punched from a 212 cm^2 foil sheet. The foils were then cleaned with acetone to ensure that the surfaces were free of any impurities. After drying they were weighed and labelled for use in the stack. Similarly copper foils with thicknesses of 0.11819 g/cm^2 and 0.04999 g/cm^2 respectively were prepared from sheets of foil. The latter thickness was used in the 40 MeV stack. All these foils were obtained from Goodfellow Metals Ltd (Cambridge, England).

3.2.4 Irradiations

Each of the various foil stacks was irradiated for 1 hour at incident proton beam energies of 100 ± 0.93 , 66.0 ± 0.86 and 40.0 ± 0.50 MeV respectively, using the external beam of the separated-sector cyclotron facility. These were done on three separate days. The 66 MeV irradiation was completed on the 11th of March 1998, while the 100 MeV and 40 MeV irradiations were executed on 27th March 1998 and 4th April 1998, respectively. The idea was to leave enough time between experiments to complete the first two counting sessions in order to count valuable short-lived isotopes before they decay to their daughters.

All three irradiations were carried out in a single stack holder and in each case the beam was stopped in a thick copper disk directly behind the stack. A schematic diagram of the experimental setup for the irradiation is shown in Figure 3-3. The beams were well-focussed and had intensities of the order of 100 nA. Fluctuations in the beam intensity were less than 5% for all the energies.

Focusing and centering of the beam was accomplished with the aid of a low intensity beam of 10 nA, a focusing unit and a television camera. The focussing unit comprises a copper beam

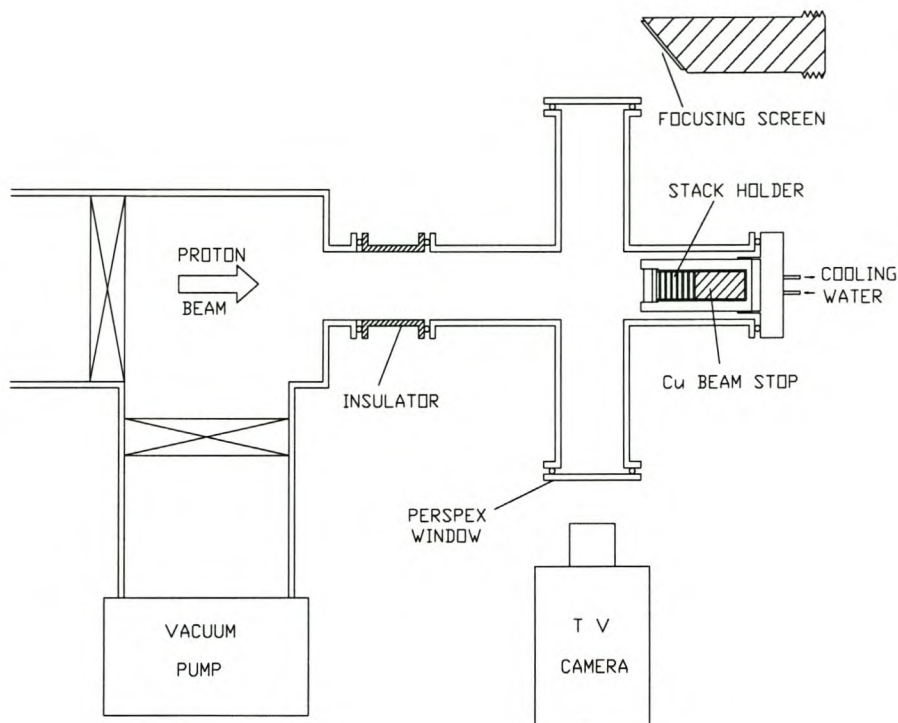


Figure 3-3: Diagram of the experimental setup for the foil stack irradiations. The stack holder was replaced with a BeO focusing screen during beam focusing.

stop with a BeO focusing screen mounted at 45° at the tip of the unit. The television camera was placed at 90° to the direction of the beam, aiming it at the BeO screen. The proton beam was directed to this setup for a few seconds to test its focusing and centering. Corrections were made where necessary and the process repeated. After focusing the unit was removed and replaced by the simple stack holder before the actual irradiation commenced. Confirmation of the focus and centering was seen in autoradiograms (Polaroid instant film pictures) that were taken afterwards from a representative foil in each stack. These autoradiograms were made by placing an irradiated foil on the instant film and marking its position. The radiation emitted from the foil exposes the film and together with the markings show the position and size of the beam spot.

3.2.5 Quantitative off-line gamma-ray spectroscopy

Immediately after each bombardment the stack was removed, disassembled and the KBr targets were individually sealed in plastic bags. This was done to prevent the possible loss of krypton gas, as well as keeping the brittle salt tablets from breaking. Gamma-ray spectroscopy started directly after this procedure.

3.2.5.1 Counting procedure.

The gamma-ray spectra of the radioactivity generated in each of the targets were recorded by the use of the experimental setup shown in Figure 3-4. Each foil was counted individually in four counting sessions. The first session started 10 minutes after the end of bombardment while the fourth was done a month later. Counting times ranged from 200 seconds for the first counting session, in order to measure short-lived isotopes, to 3600 seconds. The total dead times of the system were kept below 20% by varying the detector-to-foil distance. A summary of the counting session durations is given in Table 3.1.

Counting Session	Counting Times - live time (seconds)
1	200
2	500
3	1200
4	3600

Table 3-1 *The duration of the different counting sessions.*

Each of the copper monitor foils used in the 40 MeV stack was counted for 500 seconds about two hours after the end of bombardment. This was done to accumulate satisfactory counting statistics for ^{62}Zn which has a half-life of 9.2 h. The aluminium monitor foils were counted about one year later for the measurement of ^{22}Na activity (counting time 6 hours).

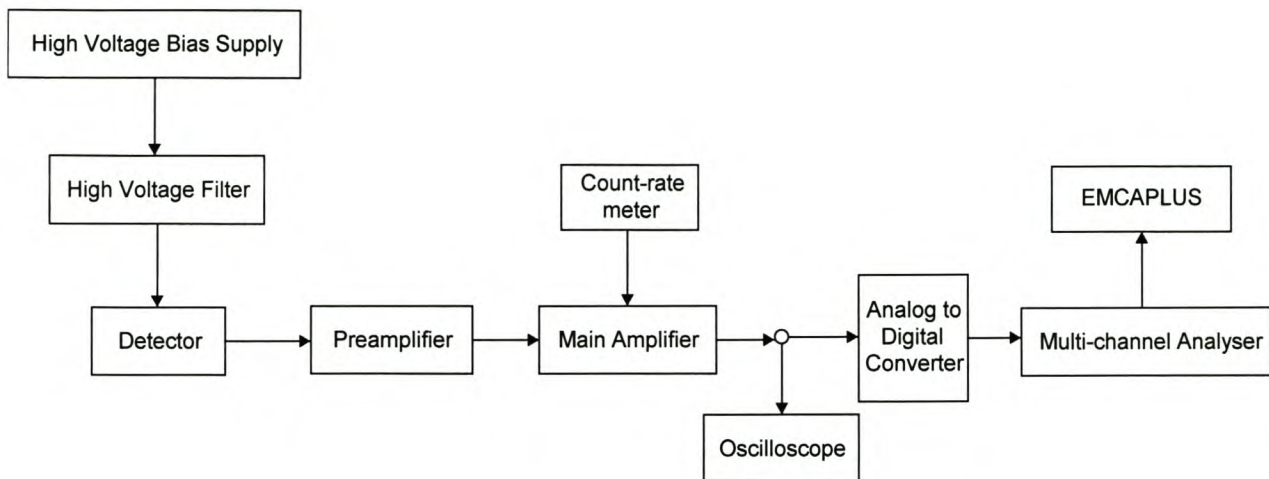


Figure 3-4: Block diagram of the electronic setup for the counting of the foils.

3.2.5.2 Detector- and electronics setup

The detector setup used for the off-line gamma-spectroscopy of the radioactive foils consisted of a 2m long bench with moveable foil holder and an intrinsic germanium detector (ORTEC HPGe detector with a thin Be window) at one end. Accurate source-to-detector distances are therefore easily set with a high degree of repeatability. This results in accurate detector efficiency values.

The detector has a resolution of 2.13 keV FWHM for the 1.33 MeV gamma ray of ^{60}Co and was coupled to a 16-k channel analyser (Silena). This system included a fast ADC with a conversion time of $3 \mu\text{s}$ and a Silena Model 7614 spectroscopy amplifier. This amplifier has a built-in circuit for the rejection of pile-up pulses, while corrections for deadtime of the amplifier and ADC are handled by a circuit in the multi-channel analyser.

3.2.5.3 Energy calibration

An ^{152}Eu reference source, with its accurately known peaks spread across the entire gamma-energy range of interest, was used to calibrate the channel numbers in terms of energy.

3.2.5.4 Efficiency calibration

As counting geometry plays a vital role in the determination of the counts in a gamma-ray peak and therefore also in the cross section value, an efficiency calibration needs to be done for those geometries used in the measurements. These values, that are in actual fact conversion factors between the number of gamma rays produced by the source and the number detected, are calculated from the activity of a reference source.

To cover the entire gamma-energy range of interest, three reference point sources were selected: ^{241}Am (13.9 - 59.5 keV), ^{133}Ba (80.9 - 383.9 keV), ^{152}Eu (121.8 - 1408.0 keV) and their individual gamma-ray spectra obtained at distances ranging from 0.15 cm to 2 m. Efficiency values were then compared with existing values and in some cases new curves (efficiency as a function of energy) were drawn (e.g. 40 cm) and used in the calculation of the cross sections.

3.2.6 Data analysis

3.2.6.1 Procedures

The characteristic gamma rays of the different radioisotopes were identified and their peak areas used in the cross section calculations.

After each foil was counted a listing of all the characteristic gamma rays together with their associated energies was made using the peak analysis software (EMCAPLUS) supplied with the Silena multi-channel analyser. The software included routines for peak integration and background subtraction, which were done automatically before the listing was compiled.

Radioisotopes were identified by using the decay data of Reus and Westmeier [Reu83] for each gamma ray. The selection to be used for the calculations was narrowed down by excluding any isotopes with a half-life of shorter than 10 minutes, or radioactive products that are not possible to produce with protons on bromine.

At first all high intensity lines of specific expected isotopes were identified. In some cases interference from other radioactive products made it necessary to use a lower intensity line. This did not always solve all the problems and hence sometimes a different counting session

was chosen for example where the interference of a short-lived isotope was no longer present due to its decay. In cases where interfering isotopes have similar decay times these isotopes were ignored. An example is the 1229.1 keV line which can either be ^{76}Kr ($T_{1/2} = 14.6$ h) or ^{76}Br ($T_{1/2} = 16.0$ h).

The peak areas for those isotopes showing no interference from other isotopes were then used in the calculation of the cross section and yield values, making use of the equations outlined in Appendix B. A tabulation of these isotopes together with their nuclear decay data used [Reu83] is given in Table 3-2.

Counting Session	Isotope	Half-life	Energy (keV) of γ used	Intensity (%)
1				
	^{75}Br	1.62 h	286.6	92.0
	^{77}Kr	1.24 h	129.7	80.0
2				
	^{80m}Br	4.42 h	37.1	39.1
	^{76}Kr	14.8 h	315.7	40.0
	^{73}Se	7.15 h	361.2	97.0
3				
	^{74}As	17.78 d	595.8	60.3
	^{77}Br	2.38 d	817.8	2.15
	^{79}Kr	35.04 h	261.3	12.7
	^{71}As	2.70 d	174.9	83.1
4				
	^{72}Se	8.40 d	834.0	91.3
	^{75}Se	119.8 d	264.4	59.1

Table 3-2 *Isotopes identified for measurement in this work and their nuclear decay data used for the determination of cross section values.*

3.2.6.2 Uncertainties

When the accuracy of measured values is needed it is also important to know their uncertainties. In this study the sources contributing to the uncertainties in the cross sections and energy values were identified.

3.2.6.2.1 Experimental uncertainty in the cross sections

The total uncertainties in the cross sections due to the experimental procedure were estimated by summing the contributing uncertainties in quadrature. They consist of a part that varies from foil to foil (with a maximum of 39.0%) and a constant part of 8.1%. Uncertainty in beam loss corrections and the counting statistics contribute to the variable part while the constant part consists of uncertainties in the detector efficiency (5%), decay corrections (1%), counting geometry (1%), foil thicknesses (1%), beam current integration (6%) and the uncertainty in the peak fitting of the photopeak (1%) [Ste90a]. Table 3-3 summarises these contributions to the experimental uncertainty.

Constant Part	Percentage	Variable Part	Percentage
Detector Efficiency	5 %	Beam loss Correction	variable
Decay Correction	1 %	Counting Statistics	variable
Counting Geometry	1 %		
Foil Thickness	1 %		
Beam current Integration	6 %		
Peak fitting of Photopeak	1 %		
Statistical Total	8.1 %	Statistical Total	max 39.0 %

Table 3-3 *Summary of the contributions to the experimental uncertainty in cross section values obtained in this work.*

3.2.6.2.2 Uncertainties in the energy values

Not only are the cross sections subject to uncertainty, but their associated proton energy values as well. Here the contributions are the uncertainties in the foil thicknesses, stopping powers

and incident proton energies [Nor90]. It was estimated that this uncertainty should be less than 1.0 MeV for all the data points. In the case of the 66 MeV and 40 MeV stacks this estimation was proven wrong when the calculated incident proton energies for the monitor foils were compared with the proton energies of the published monitor foil data. At some data points this energy shift was more than 2.4 MeV. Although all parameters were rechecked, the origin of this discrepancy could not be found. Therefore the energy values were corrected with the aid of the published monitor foil data. The correction is described in § 3.2.6.4. Adjustments to the 100 MeV stack were not necessary as a good comparison was seen between the measured and published monitor excitation functions.

3.2.6.2.3 Other sources of uncertainty

The energy straggling in the foil stack and the proton beam energy spread also influence the accuracy of the data. A correction could not be made, but a significant influence on the results is not expected [Nor90].

3.2.6.3 Proton flux measurements

To increase the accuracy of the cross sections, the uncertainty in the total incident proton flux should be as small as possible. Two methods are commonly used to measure this parameter.

3.2.6.3.1 Direct measurement

This method relies on the direct measurement of the proton flux by integrating the beam current. This is accomplished by collecting charge by means of a Faraday-cup arrangement (prevent secondary electrons from escaping) and a current integrator which registers the total charge collected. Since a proper Faraday cup was not used in the present work only an approximate proton flux was obtained by direct measurement.

3.2.6.3.2 Monitor reactions

When a properly designed Faraday-cup is not available a monitor reaction of which the excitation function is accurately known is used to determine the proton flux. Monitor foils of the

appropriate material are then included in each of the foil stacks. After the irradiation the residual activity of the radioisotope of interest produced in the monitor foils is used to determine the actual proton flux incident on the stack.

In this work accurate direct measurement could not be done and hence the excitation functions for the production of ^{22}Na and ^{62}Zn via the $^{27}\text{Al}(p,x)^{22}\text{Na}$ and $^{nat}\text{Cu}(p,x)^{62}\text{Zn}$ reactions were selected as monitor reactions. The $^{nat}\text{Cu}(p,x)^{62}\text{Zn}$ reaction was used for the energy range below 25 MeV. Aluminium and copper monitor foils were used for this purpose and were included in the stacks. Following the irradiation the relevant radioactivities in the Al and Cu foils were gamma spectroscopically analysed and the approximate cross sections were calculated using the approximate proton flux obtained by direct measurement. They were then compared with published cross section values [Mil92].

The approximate monitor cross section data obtained in this study using the integrated beam current are listed in Appendix C and graphically compared with the published values in Figures 3-5 and 3-7. From these figures, a shift in energy and cross section (related to the proton flux) are clearly seen in the case of the 40 and 66 MeV stacks. Adjustments were made first to the energy values and then to the approximate proton flux (see § 3.2.6.4) and the results are shown in Figures 3-6, 3-8 and 3-9. The approximate proton flux as measured by the integration of the beam current was regarded as accurate in the case of the 100 MeV stack and no adjustments were made. These new energy and proton flux values were then used in the calculation of cross section and yield values.

3.2.6.4 Energy and proton flux adjustments from the monitor reactions

Adjustments in the energy values as well as the approximate proton flux were necessary in the case of the 40 and 66 MeV stacks. Corrections were made according to the comparison between the published and the measured monitor excitation functions.

The energy shift in each of the two stacks was corrected by using a fitting function to recalculate the incident energies on each foil. This fitting function was obtained by the following operations: Five energy differences (between the energy values of this work and the published values) were selected at random and plotted as a function of energy. A best fit procedure was

then applied to these points resulting in a fitting function. These functions, together with the original and new energy values, are given in Appendix C.

Following the energy shift correction, both the proton fluxes (as measured with the current integrator) were adjusted by comparing the maxima of the published and new experimental monitor excitation functions (see Figures 3-5 and 3-7). In the case of the 40 MeV stack it was necessary to multiply the proton flux with a factor of 1.07 for the maxima to coincide. The maxima of the two excitation functions of the 66 MeV stack corresponded when the proton flux was multiplied with a factor of 1.06. The original and new cross section values for the measured monitor excitation function are given in Appendix C.

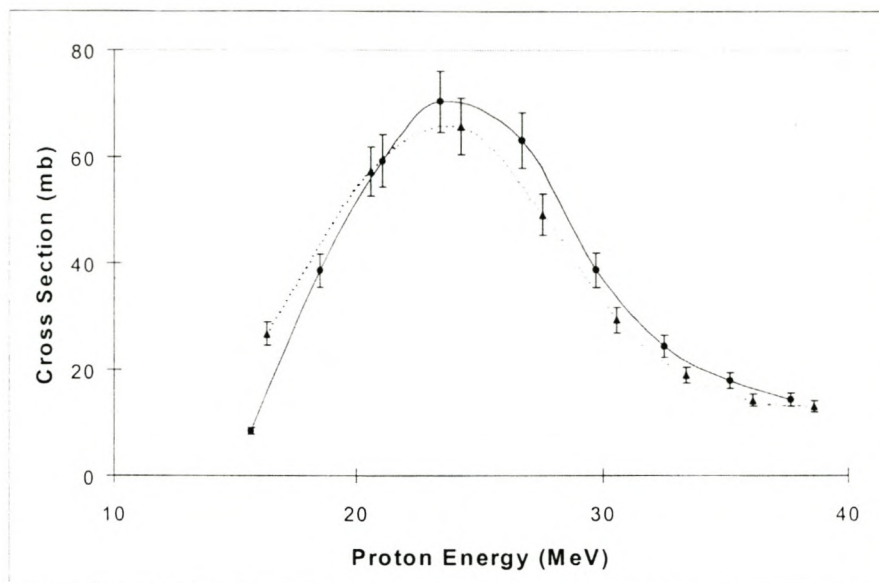


Figure 3-5: The comparison between the experimental excitation functions for the production of ^{62}Zn in the bombardment of Cu with protons before the adjustments: solid line, this work; broken line Mills, et al. [Mil92].

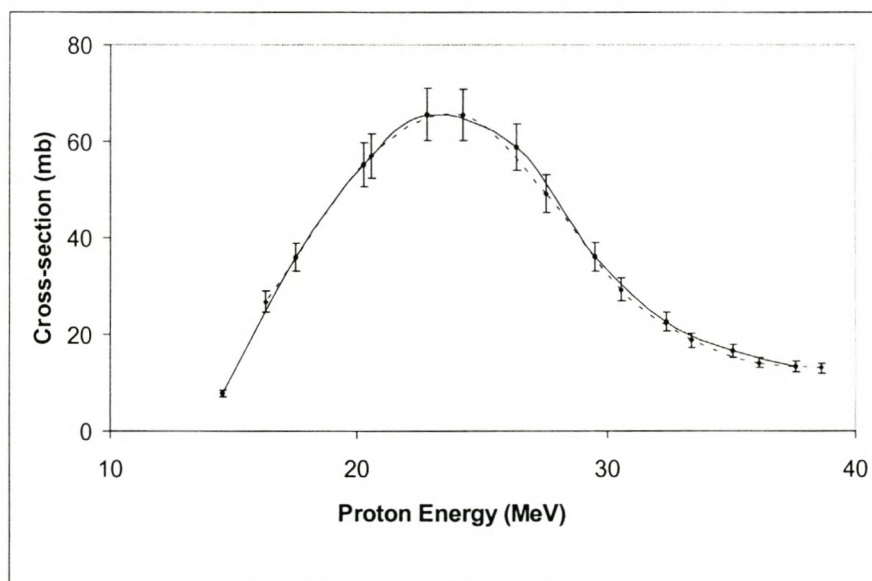


Figure 3-6: The comparison between the experimental excitation functions for the production of ^{62}Zn in the bombardment of Cu with protons after the adjustments: solid line, this work; broken line Mills, et al. [Mil92].

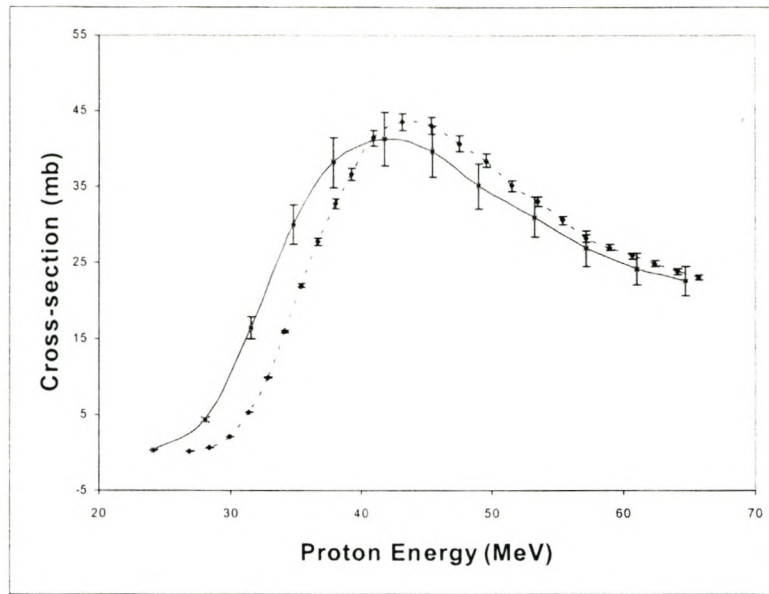


Figure 3-7: The comparison between the experimental excitation functions for the production of ^{22}Na in the 66 MeV stack before any adjustments: solid line, this work; broken line Steyn, et al. [Ste90].

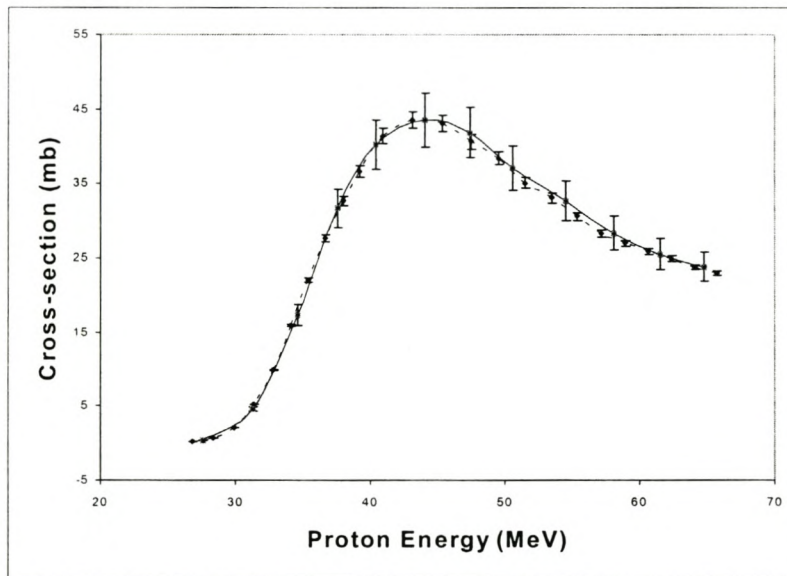


Figure 3-8: The comparison between the experimental excitation functions for the production of ^{22}Na in the 66 MeV stack after the adjustments: solid line, this work; broken line Steyn, et al. [Ste90].

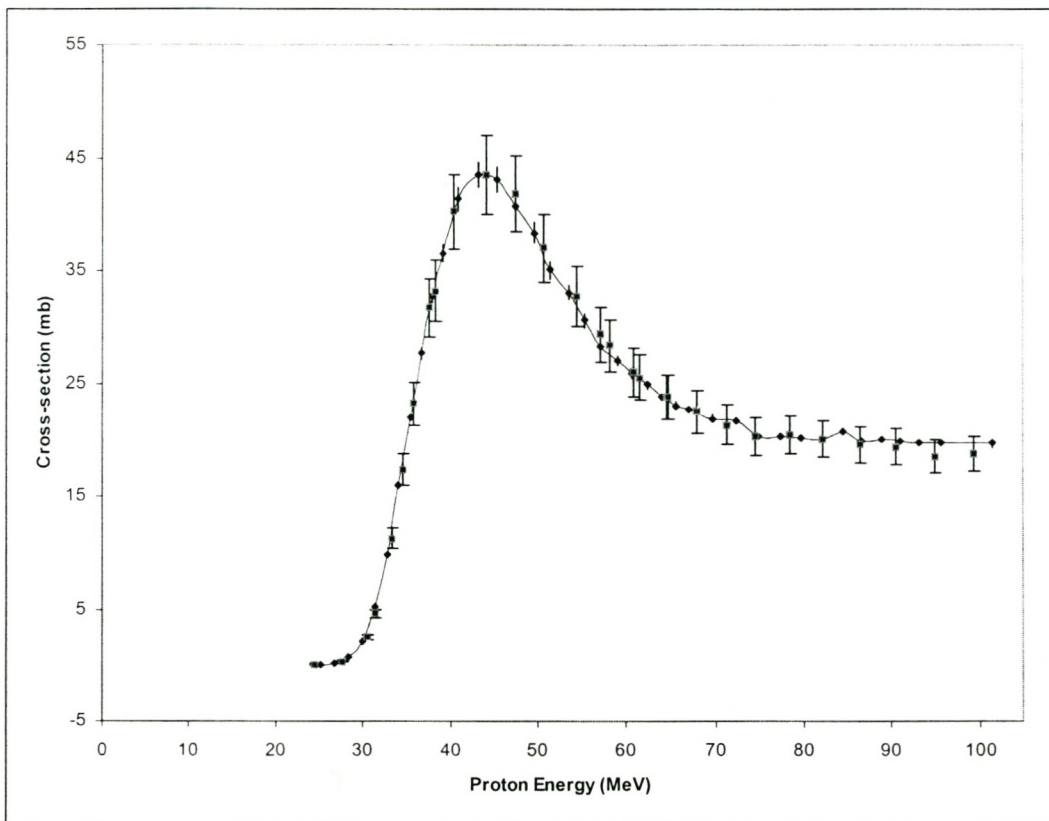


Figure 3-9: The comparison between the experimental excitation functions for the production of ^{22}Na in the bombardment of Al with protons (66 and 100 MeV stacks): this work (■) and Steyn, et al.(◆ with solid line to guide the eye) [Ste90].

Chapter 4

Results and discussion

4.1 Introduction

This study focuses on the measurement of excitation functions in the energy range below 100 MeV when potassium bromide, as target material, is bombarded with a proton beam. From these results, special attention is given to the production of selenium-75. A total of 11 excitation functions were measured by means of the stacked-foil experiments described in Chapter 3. The results thereof as well as the thin and thick target yields of the three observed selenium radioisotopes ($^{72,73,75}\text{Se}$), determined from the cross section values, are presented in this chapter. The measured cross section values are given in Appendix D.

4.2 Selenium isotopes

4.2.1 Excitation functions

As this is a new production route for ^{75}Se via ^{nat}Br nuclear reactions, no previous data could be found in the literature for comparison purposes. This is also the case for the other two selenium isotopes of interest, ^{72}Se and ^{73}Se , measured in this study. These three excitation functions are presented in Figures 4-1, 4-5 and 4-6.

Selenium-75 can be produced by the decay-chain of the radioisotopes ^{75}Kr to ^{75}Br to ^{75}Se . Krypton-75 can be produced directly by $^{79}\text{Br}(p,5n)$ and $^{81}\text{Br}(p,7n)$ nuclear reactions, ^{75}Br is

produced directly via $^{79}\text{Br}(p,p4n)$ and $^{81}\text{Br}(p,p6n)$ and ^{75}Se via $^{79}\text{Br}(p,2p3n)$, $^{81}\text{Br}(p,2p5n)$, $^{79}\text{Br}(p,\alpha n)$ and $^{81}\text{Br}(p,\alpha 3n)$ nuclear reactions. As seen in Figure 4-1 the maximum cross section for the production of ^{75}Se via all the possible reactions is 116.5 mb for the incident energy of 68.91 MeV.

For a better understanding of the effect of the selenium radiocontaminants in the production of ^{75}Se , the production cross section values for all three selenium isotopes ($^{72,73,75}\text{Se}$) are plotted on a logarithmic scale against incident proton energy (see Figure 4-2). From this figure it is clear that no detectable radiocontaminant is produced in the energy region between 16.1 MeV and 39.2 MeV. At a first glance the region above 39.2 MeV may look unsuitable for ^{75}Se production due to the presence of the other two selenium isotopes. However, if one takes into account that the half-life of ^{75}Se is 119.8 days [Reu83] compared to 8.40 days [Reu83] and 7.15 hours [Reu83] for ^{72}Se and ^{73}Se respectively, it is still possible to produce a pure ^{75}Se in the higher energy region by performing the chemical separation a number of weeks after the end of bombardment.

Production routes can be compared by calculating the thick target yield for a specific incident energy. This is done by determining the thin target yields from the measured cross section values and integrating it over the energy range used (see Appendix B). These yield curves, for the production of ^{75}Se , ^{73}Se and ^{72}Se , are presented in Figures 4-3 and 4-4 for a bromine and potassium bromide target.

4.2.2 Routine production at the NAC

At the NAC a 66 MeV proton beam is available for radioisotope production on a regular basis. It is therefore sensible to find (for this particular beam energy) the incident energy that will produce the maximum yield of ^{75}Se .

The thick target yield values of all three selenium isotopes, together with a range of decay times after the end of bombardment (EOB) were calculated and are given in Table 4-1. As lower energies did not show better yield values the maximum incident energy of 65.7 MeV, which is typical for a routine production target and an exit energy of 16 MeV, were used for these calculations.

Time (d)	Activity		
	⁷⁵ Se (mCi)	⁷³ Se (% of total)	⁷² Se (% of total)
0 (EOB)	0.0423	95.2	3.38
4	0.0413	0.226	63.6
10	0.0399	≈ 0	52.6
17	0.0383	≈ 0	39.3
25	0.0366	≈ 0	25.9
34	0.0347	≈ 0	14.9
71	0.0280	≈ 0	1.02
84	0.0260	≈ 0	0.378

Table 4-1: Summary of the thick target yield values for 1 μAh for the production energy window 65.7 - 16 MeV for ^{75,73,72}Se at different times after EOB.

In Table 4-1 one can see that at EOB the highest yield value belongs to ⁷³Se which accounts for 95.2% of the total selenium yield, compared to the 1.42% of ⁷⁵Se. After less than 4 days the ⁷³Se decays to less than 1% of the total activity due to its short half-life.

During the above-mentioned time period after EOB the ⁷⁵Se is also overshadowed by the contribution of ⁷²Se, but after 11 days the roles are reversed. After just 25 days after EOB ⁷⁵Se contributes to 74.1% of the total yield and after another 47 days the ⁷²Se is, for all practical purposes, no longer present as its activity is less than 1% of the total activity.

The yield for ⁷⁵Se is expected to be 0.0423 mCi/ μAh at EOB. By waiting 72 days after EOB, a production rate of 0.0280 mCi/ μAh is obtained. This value is more than twice the thick target yield of 0.012 mCi/ μAh for the ⁷⁵As(p,n) process [Ble94] discussed in § 3.2.3. From Table 4-1 it is seen that this yield value will change according to the desired value of ⁷²Se (and ⁷³Se during the first 4 days) contamination in the final product.

4.3 Comparison

4.3.1 Theoretical calculation of excitation functions

Theoretical cross sections were calculated for the various excitation functions for comparison with the experimental data. For this purpose the most recent version of the computer code ALICE. ALICE (IPPE) was used. Although ALICE is not regarded as the most accurate code [Nor90], agreement between experimental and theoretical values are normally expected to be within a factor of two [Ste90b].

The calculations used a single parameter set based on well established values (presented in Appendix E). No attempt was made to improve the overall agreement with the experimental data by varying these parameters. Thus the intention in this study was to apply the ALICE (IPPE) code as a "black box". As the work presented in this study was approached and performed from an applied point of view, a detailed discussion of the nuclear models and reaction mechanisms used in ALICE is considered beyond the scope of this study.

4.3.2 Published experimental excitation function data

Only four sets of data were found in the literature for comparison purposes: Diksic et al. [Dik79], De Jongh, Brinkman and Linder [Dej79], Colle and Kishore [Col74] and Blosser and Handley [Blo55]. The data points of Diksic et al. [Dik79] were published for enriched ^{79}Br and ^{81}Br targets. Although the other authors [Dej79], [Col74] and [Blo55] used natural targets, it appears that they present their data points for enriched targets without explicitly stating this fact.

All the data point values for enriched targets were adjusted in order to compare them with this study's results: For each proton energy the corresponding two cross section values were multiplied by the natural abundance of the relevant isotope (0.5069 and 0.4931 for ^{79}Br and ^{81}Br respectively) and then added. The excitation functions obtained in this way from the literature values are presented in Figures 4-7 to 4-12 and compared with the measurements done in this study. Note that our measurements include the systematic uncertainty of 8.1% as discussed in §3.2.6.2.1.

The data of Diksic et al. (\blacktriangle) [Dik79] showed good agreement with the measurement of this work in the cases of ^{76}Kr (Figure 4-10), ^{77}Kr (Figure 4-11) and ^{79}Kr (Figure 4-12). In the data set for ^{75}Br (Figure 4-7) the points at the steep slope seems to be shifted towards lower energies, but the points above 70 MeV show good agreement. In the case of ^{80m}Br (Figure 4-9) the opposite is observed: the points on the slope show good agreement while the cross section values above 30 MeV are significantly higher than the present measurements. However, the shapes of the excitation functions are similar. The agreement of the ^{77}Br (Figure 4-8) data set is satisfactory.

Data for ^{77}Kr published by De Jongh, Brinkman and Linder (\blacksquare) [Dej79] are consistently lower than the measurements obtained in this work. The same behavior is seen in their data set for ^{76}Kr , although a better agreement is seen at the positive slope of the excitation function. In the case of ^{75}Br the points seem to be shifted towards lower energies and a significant scatter in their data is apparent. The maximum cross section also appears to be slightly higher than this study's measurements.

Colle and Kishore's [Col74] published data points for ^{79}Kr show very good agreement with our measured values in the region of overlap of the data sets.

The single data point for ^{79}Kr of Blosser and Handley (\triangle) [Blo55] lies higher than the values of Colle and Kishore [Col74] but, taking into account the experimental error, the agreement is still satisfactory.

No published data could be found for the arsenic isotopes ^{71}As and ^{74}As . These excitation functions are presented in Figures 4-13 and 4-14.

The values obtained in the theoretical calculations with ALICE (IPPE) are also presented. In the cases of ^{75}Se , ^{77}Br , ^{77}Kr and ^{71}As good agreement is seen particularly with regards to the shapes of the excitation functions, with an excellent fit between theory and experiment in the case of ^{79}Kr . For ^{80m}Br the tail region of ALICE (IPPE) lies higher than our experimental values, since the code cannot calculate the contributions to metastable states so that the ALICE (IPPE) values are for the sum of the ground and metastable states ($^{80m+g}\text{Br}$). The reason for the pickup at the tip of the tail is not clear. Satisfactory agreement is seen in the excitation

functions of ^{74}As , ^{76}Kr and ^{75}Br notwithstanding the fact that an exact experimental shape was not reproduced. For the excitation functions of ^{72}Se and ^{73}Se ALICE (IPPE) predicted a shape similar to the measurements, although there appears to be a shift in the cross section values towards higher energies. One also see that the ALICE values are higher in the case of ^{72}Se and lower in the case of ^{73}Se .

In general the absolute values of the calculations agreed within a factor of two with the experimental measured values. Especially the shapes of the excitation functions are very well reproduced by ALICE (IPPE).

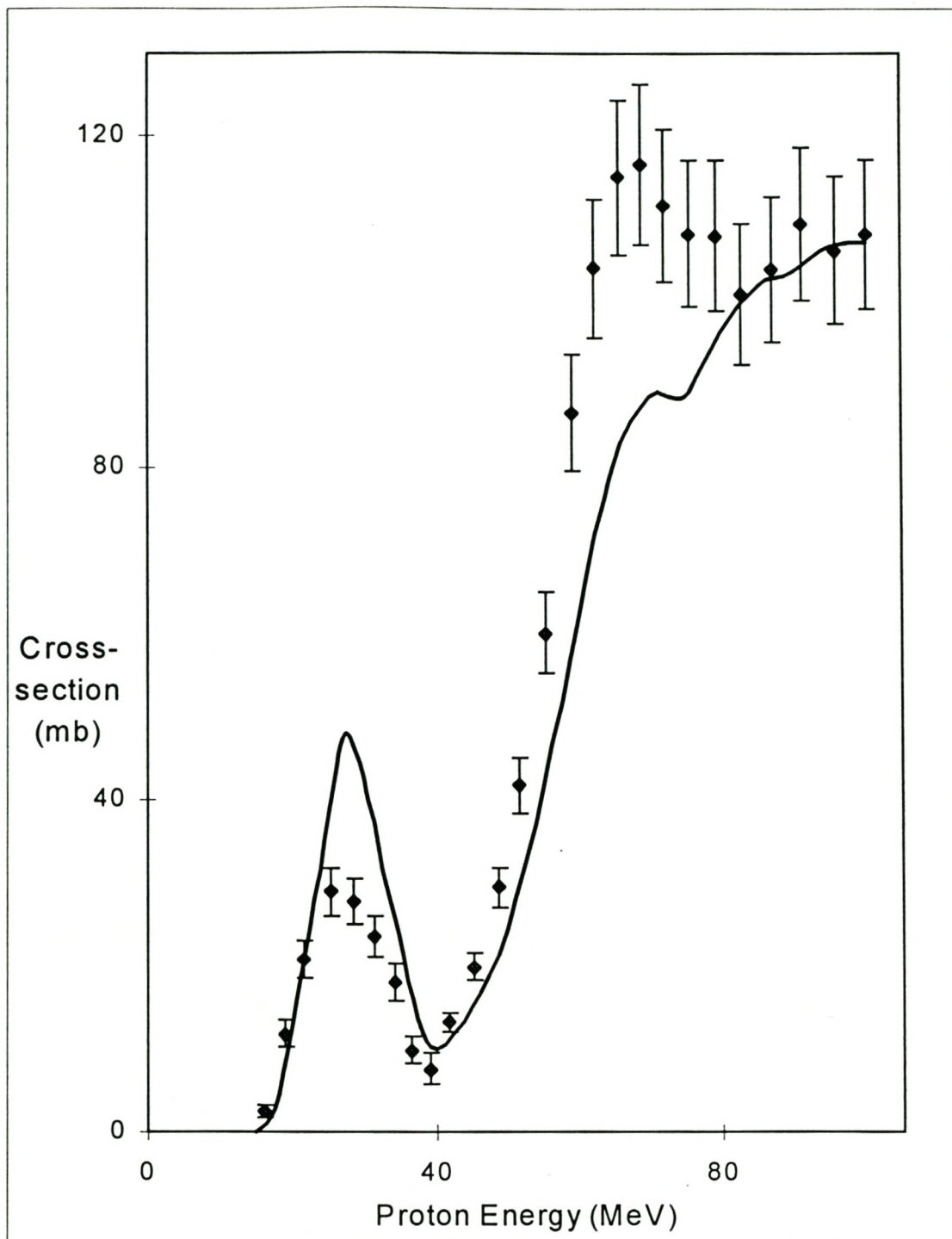


Figure 4-1: Experimental excitation function for the production of ^{75}Se in the bombardment of ^{nat}Br with protons and the theoretical calculations of Alice (solid line).

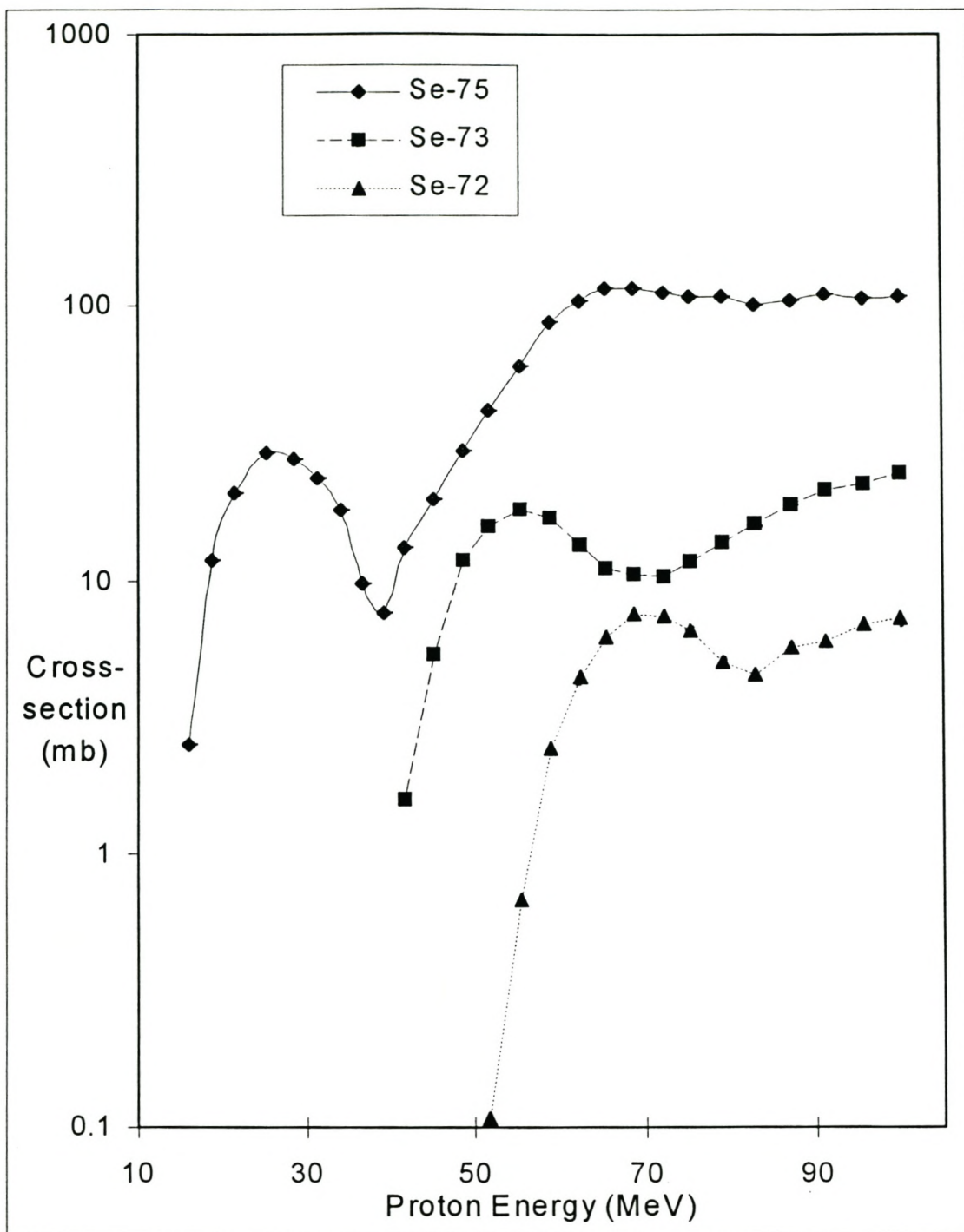


Figure 4-2: Comparison between the three experimental excitation functions for the production of the selenium isotopes ⁷⁵Se(◆), ⁷³Se(■) and ⁷²Se(▲) (curves are used to guide the eye).

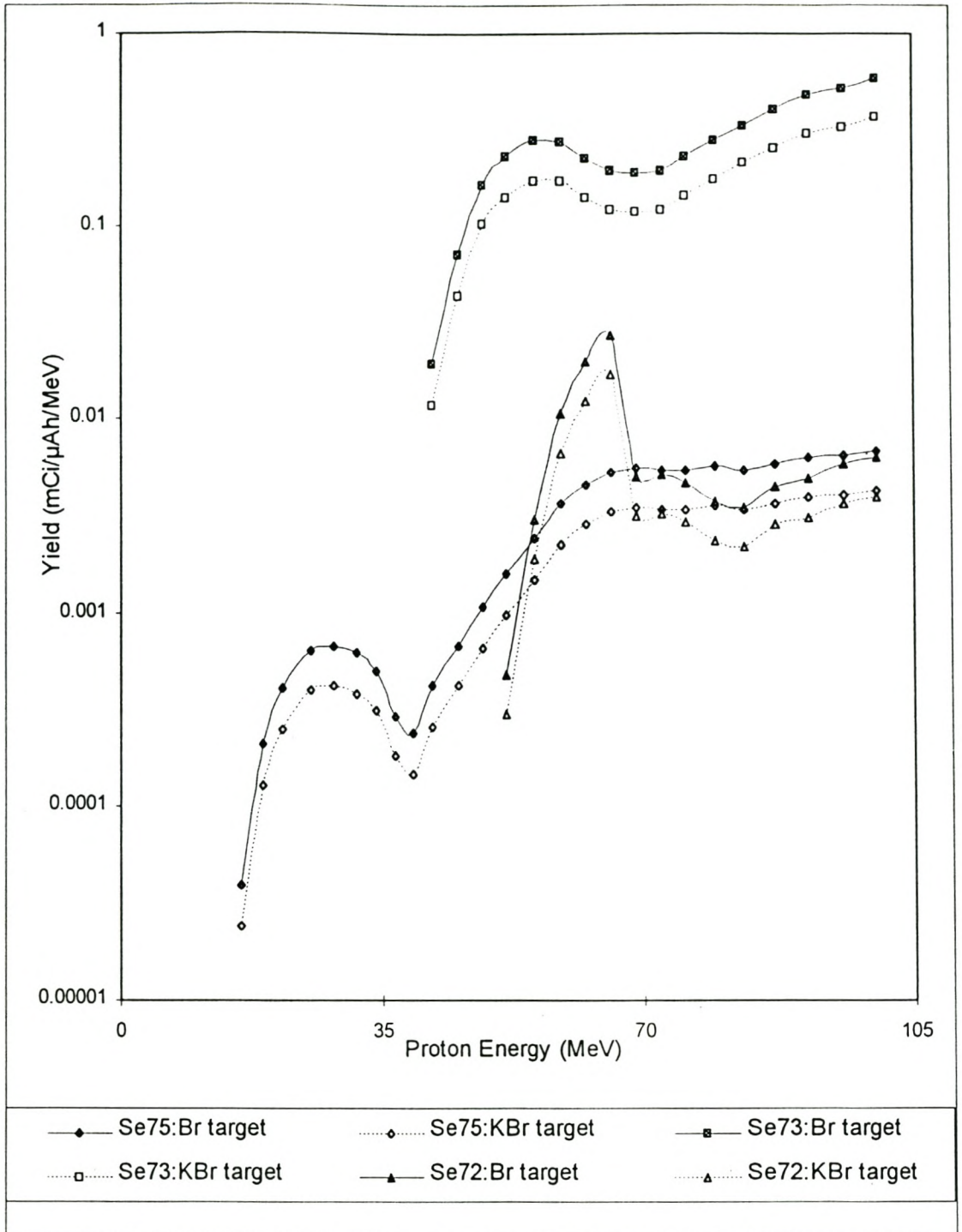


Figure 4-3: Thin target yield curves determined from the measured ^{75}Se , ^{73}Se and ^{72}Se excitation functions for Br and KBr targets at EOB.

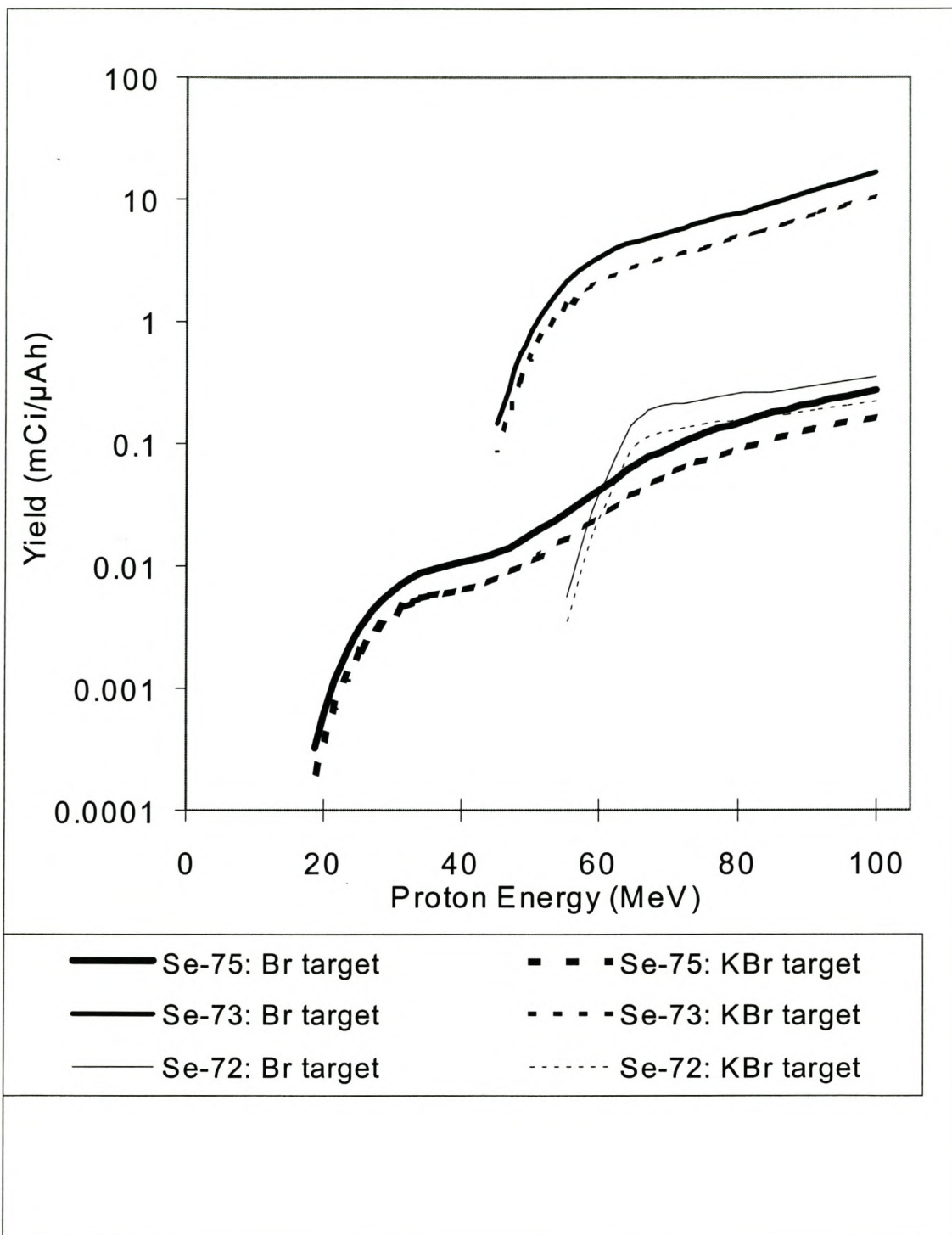


Figure 4-4: Thick target yield curves determined from the measured ^{75}Se , ^{73}Se and ^{72}Se excitation functions for Br and KBr targets at EOB.

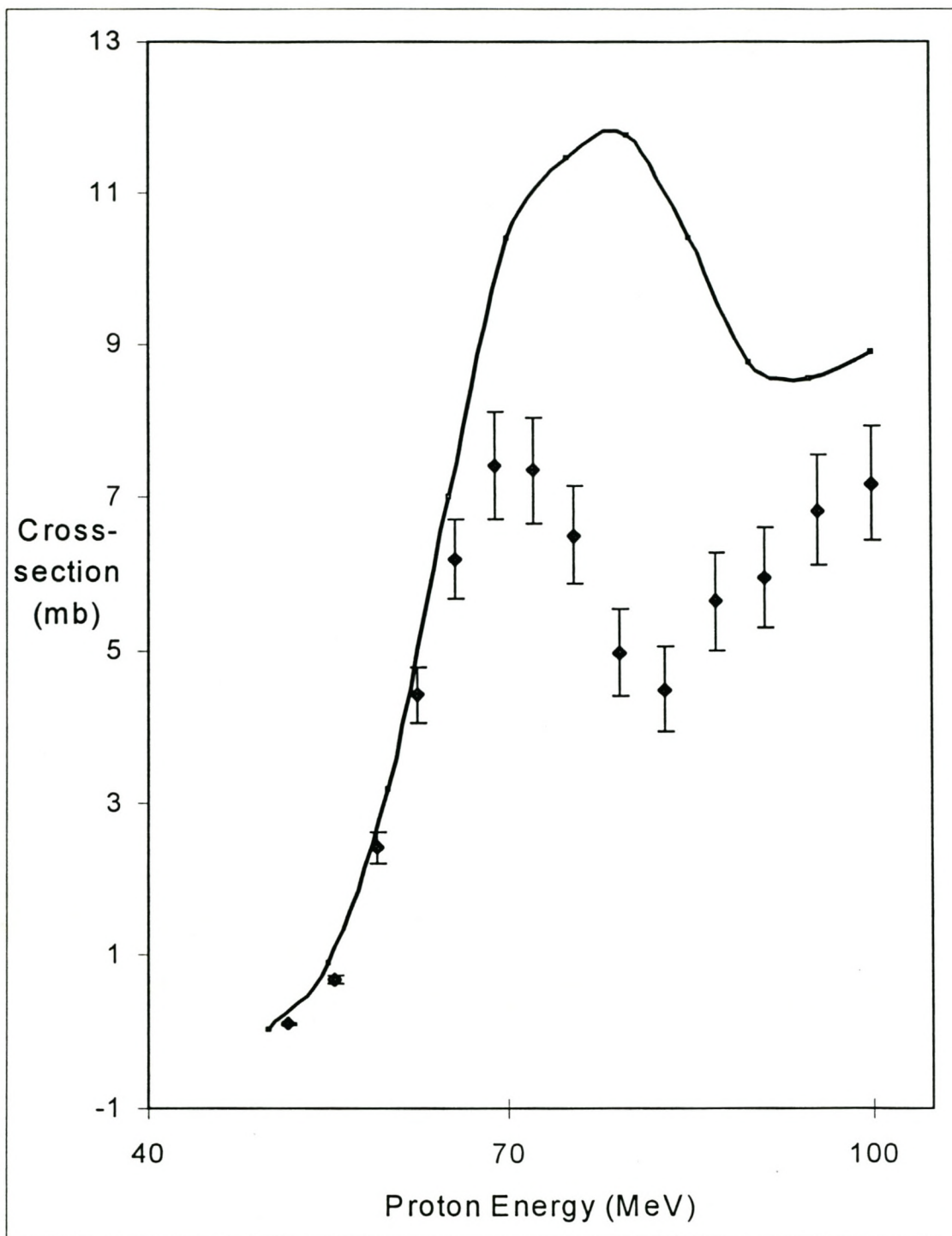


Figure 4-5: Experimental excitation function for the production of ^{72}Se in the bombardment of ^{nat}Br with protons and the theoretical calculations of Alice (solid line).

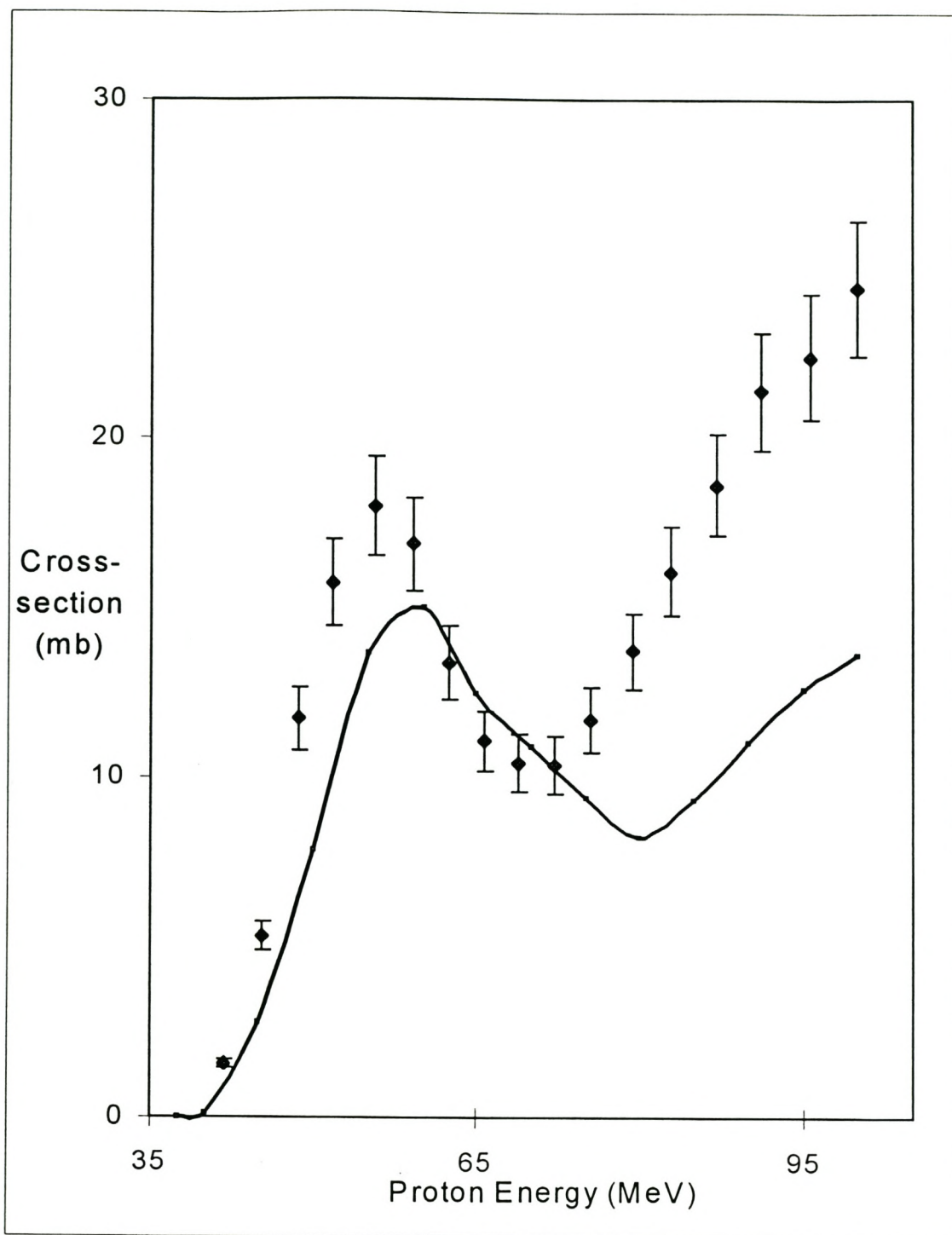


Figure 4-6: Experimental excitation functions for the production of ^{73}Se in the bombardment of ^{nat}Br with protons and the theoretical calculations of Alice (solid line).

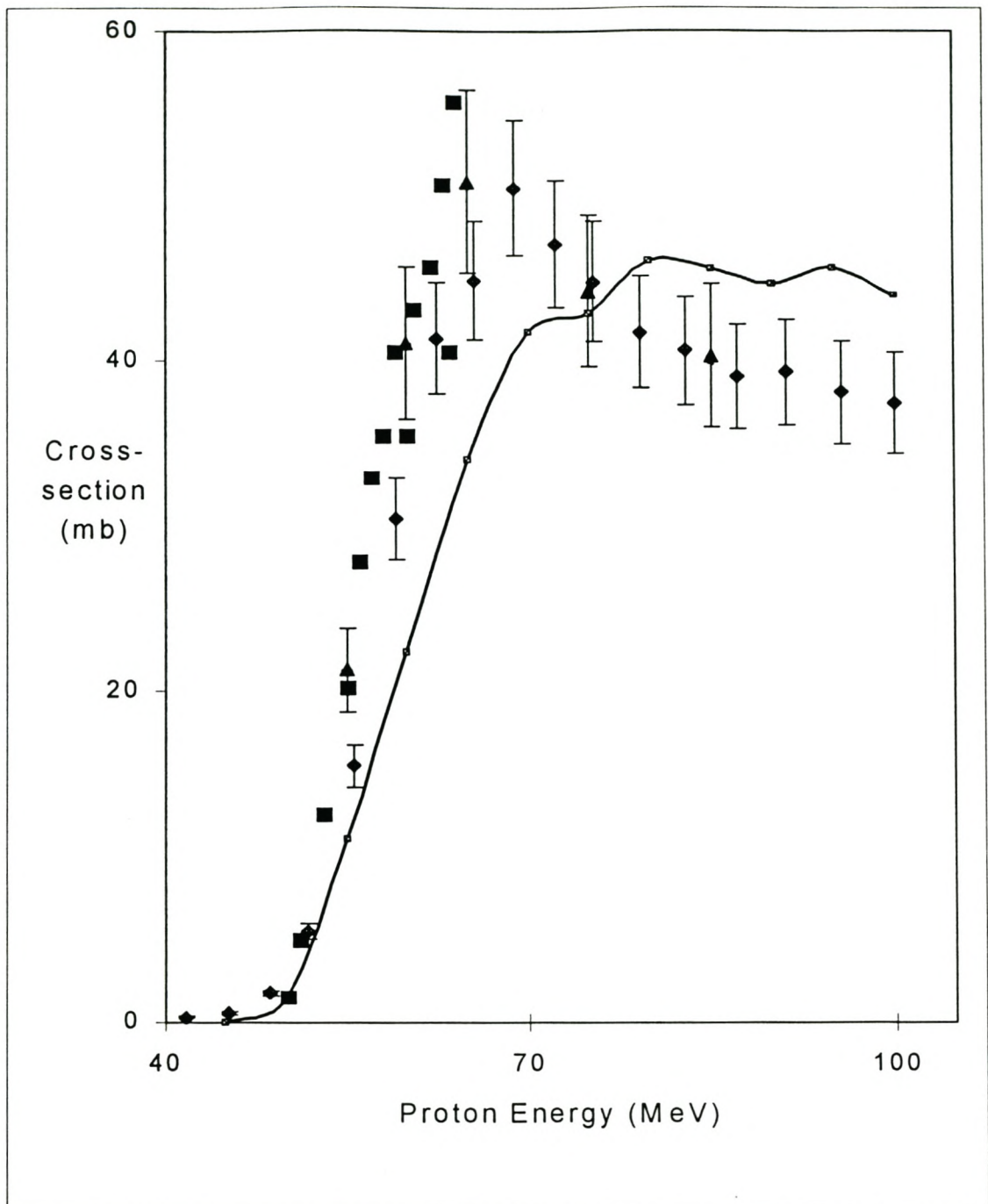


Figure 4-7: A comparison of the experimental excitation functions obtained in this work (\blacklozenge) for the production of ^{75}Br in the bombardment of ^{nat}Br with protons and data published by De Jongh, Brinkman and Linder (\blacksquare)[Dej79], Diksic et al. (\blacktriangle)[Dik79] and the theoretical calculations of Alice (solid line).

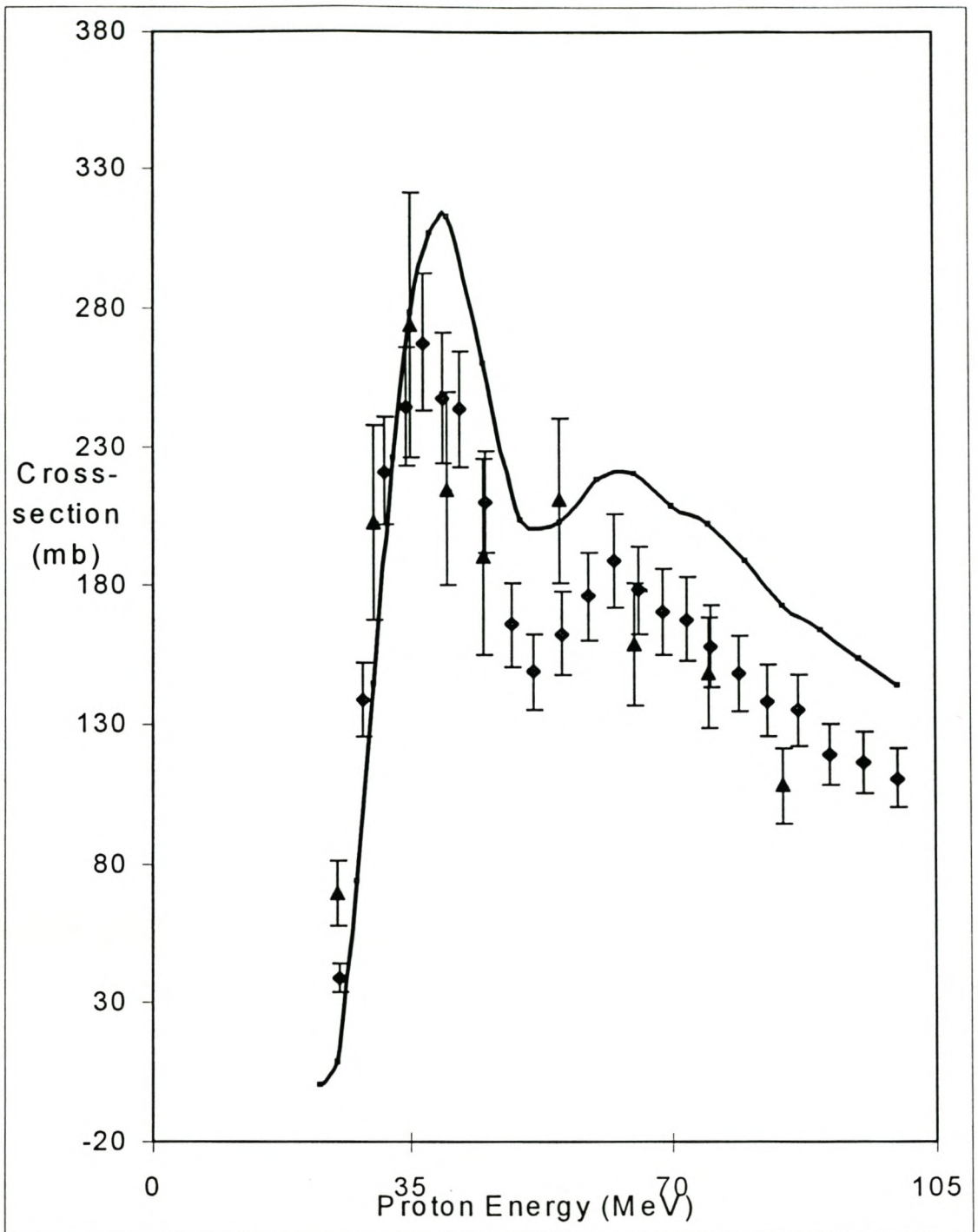


Figure 4-8: A comparison of the experimental excitation functions obtained in this work (◆) for the production of ^{77}Br in the bombardment of ^{nat}Br with protons and data published by Diksic et al. (▲)[Dik79] and theoretical calculations of Alice (solid line).

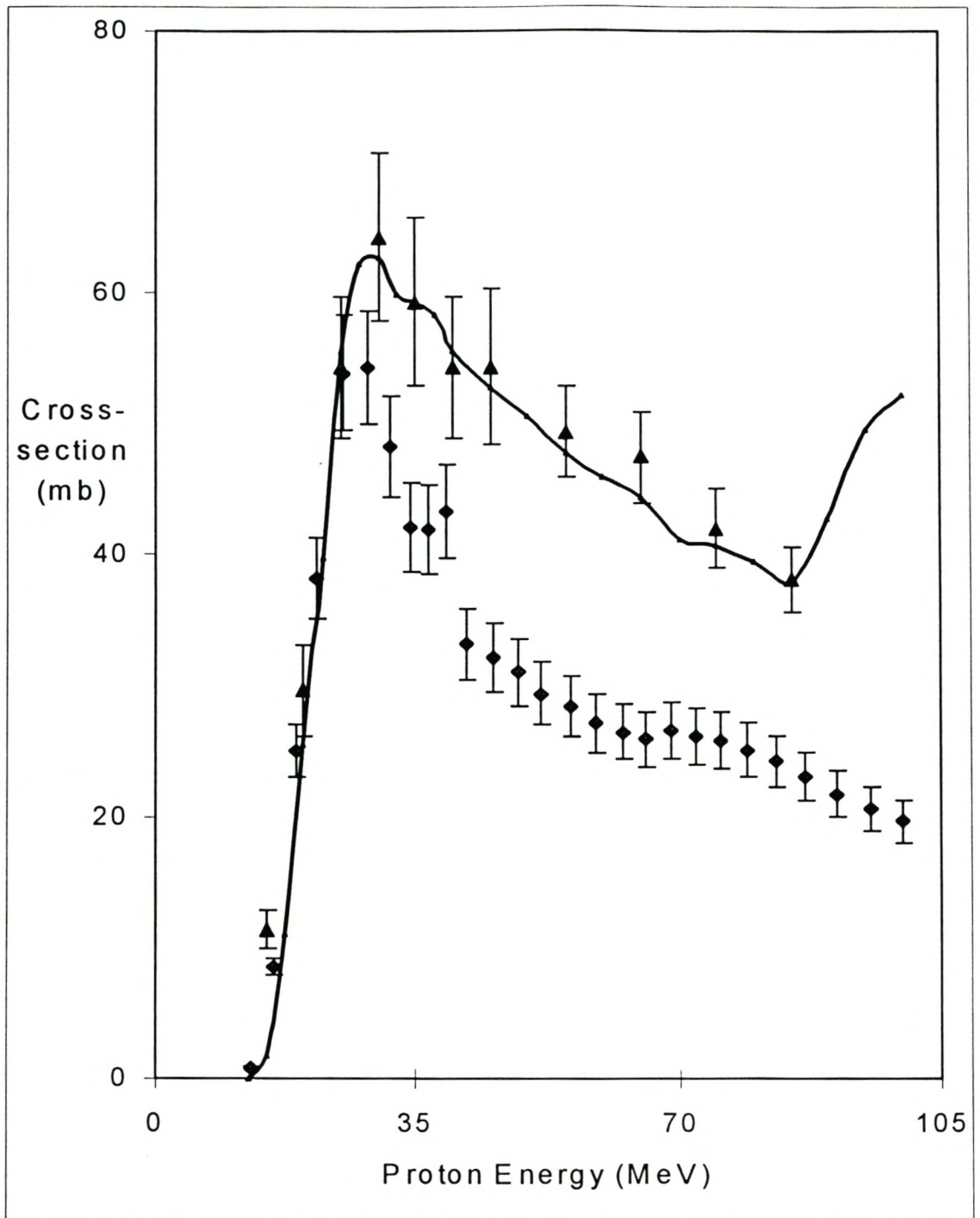


Figure 4-9: A comparison of the experimental excitation functions obtained in this work (◆) for the production of ^{80m}Br in the bombardment of ^{nat}Br with protons and data published by Diksic et al. (▲)[Dik79] and theoretical calculations of Alice (solid line).

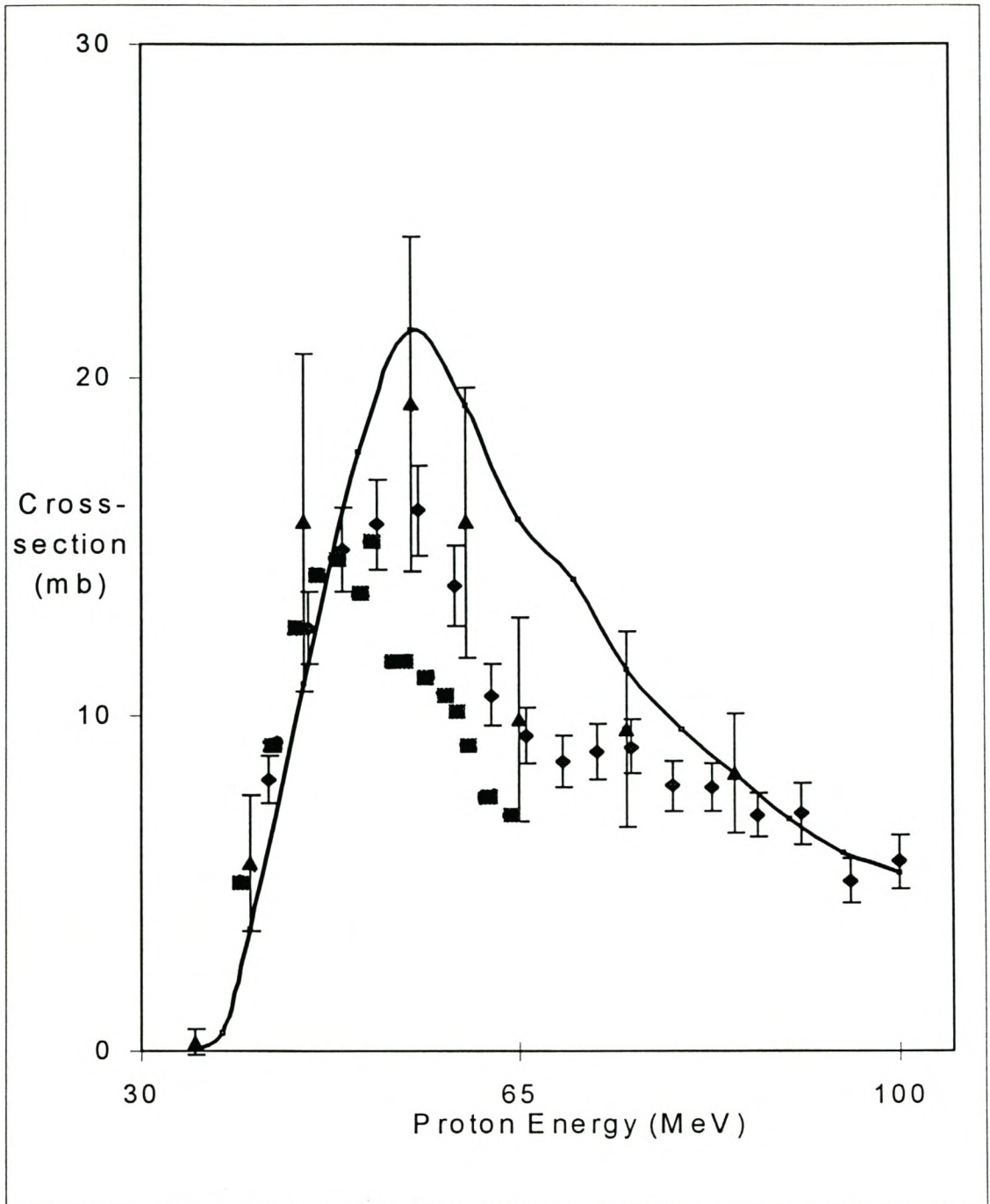


Figure 4-10: A comparison of the experimental excitation functions obtained in this work (◆) for the production of ^{76}Kr in the bombardment of ^{nat}Br with protons and data published by De Jongh, Brinkman and Linder (■)[Dej79], Diksic et al. (▲)[Dik79] and the theoretical calculations of Alice (solid line).

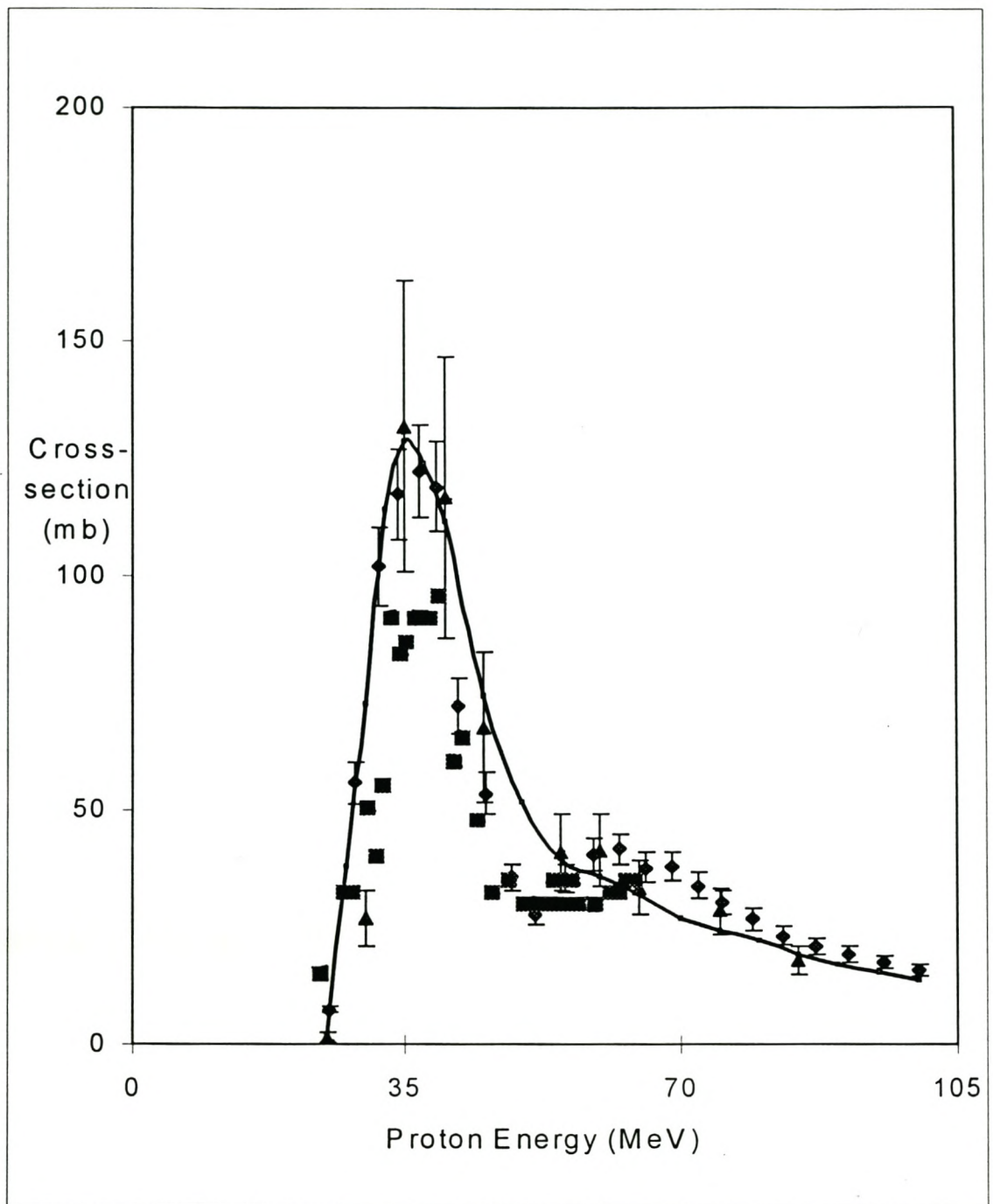


Figure 4-11: A comparison of the experimental excitation functions obtained in this work (◆) for the production of ^{77}Kr in the bombardment of ^{nat}Br with protons and data published by De Jongh, Brinkman and Linder (■)[Dej79], Diksic et al. (▲)[Dik79] and the theoretical calculations of Alice (solid line).

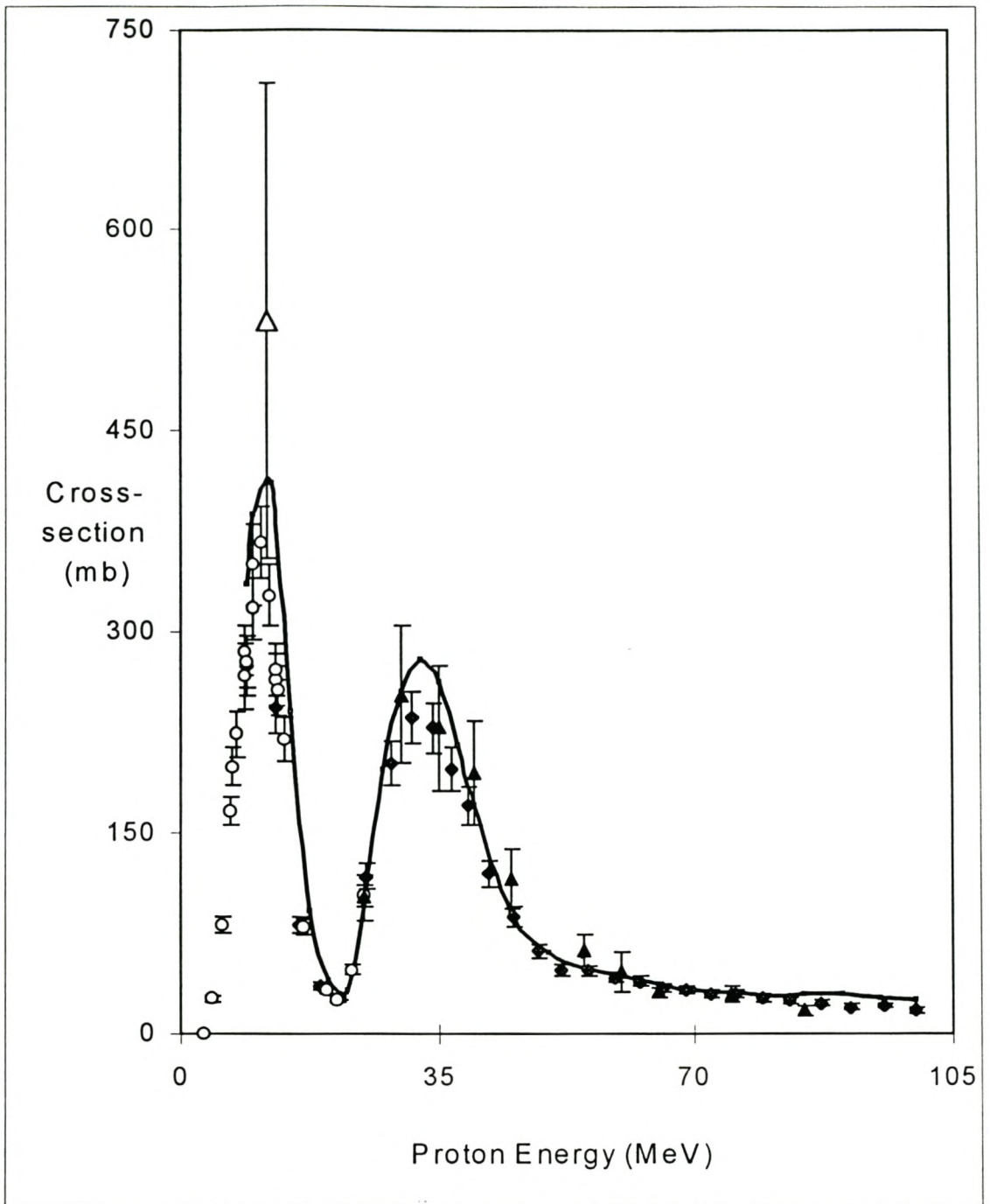


Figure 4-12: A comparison of the experimental excitation functions obtained in this work (◆) for the production of ^{79}Kr in the bombardment of ^{nat}Br with protons and data published by Diksic et al. (▲)[Dik79], Colle and Kishore (○)[Col74], Blosser and Handley (△) [Blo55] and the theoretical calculations of Alice (solid line).

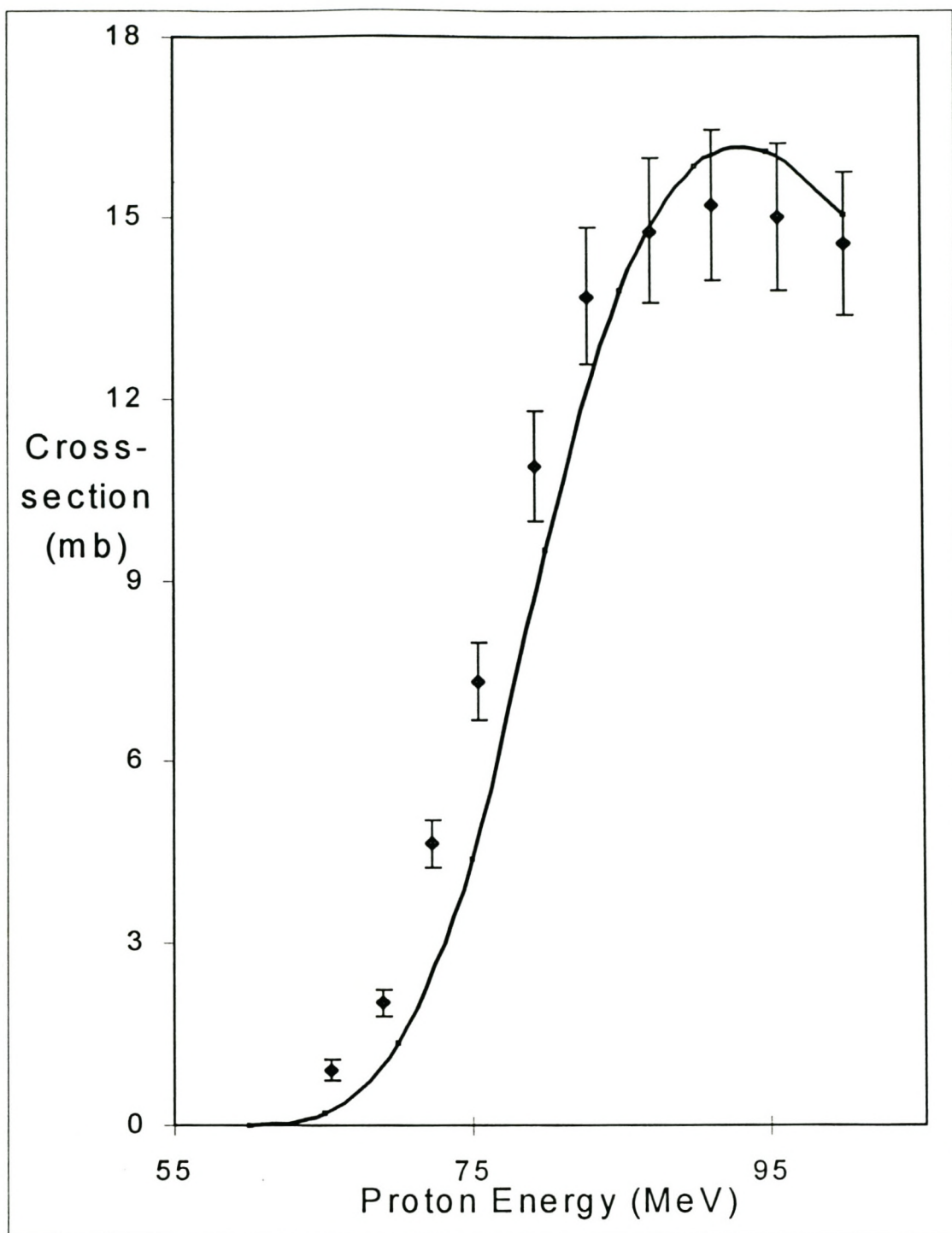


Figure 4-13: Experimental excitation functions for the production of ^{71}As in the bombardment of ^{nat}Br with protons and the theoretical calculations of Alice (solid line).

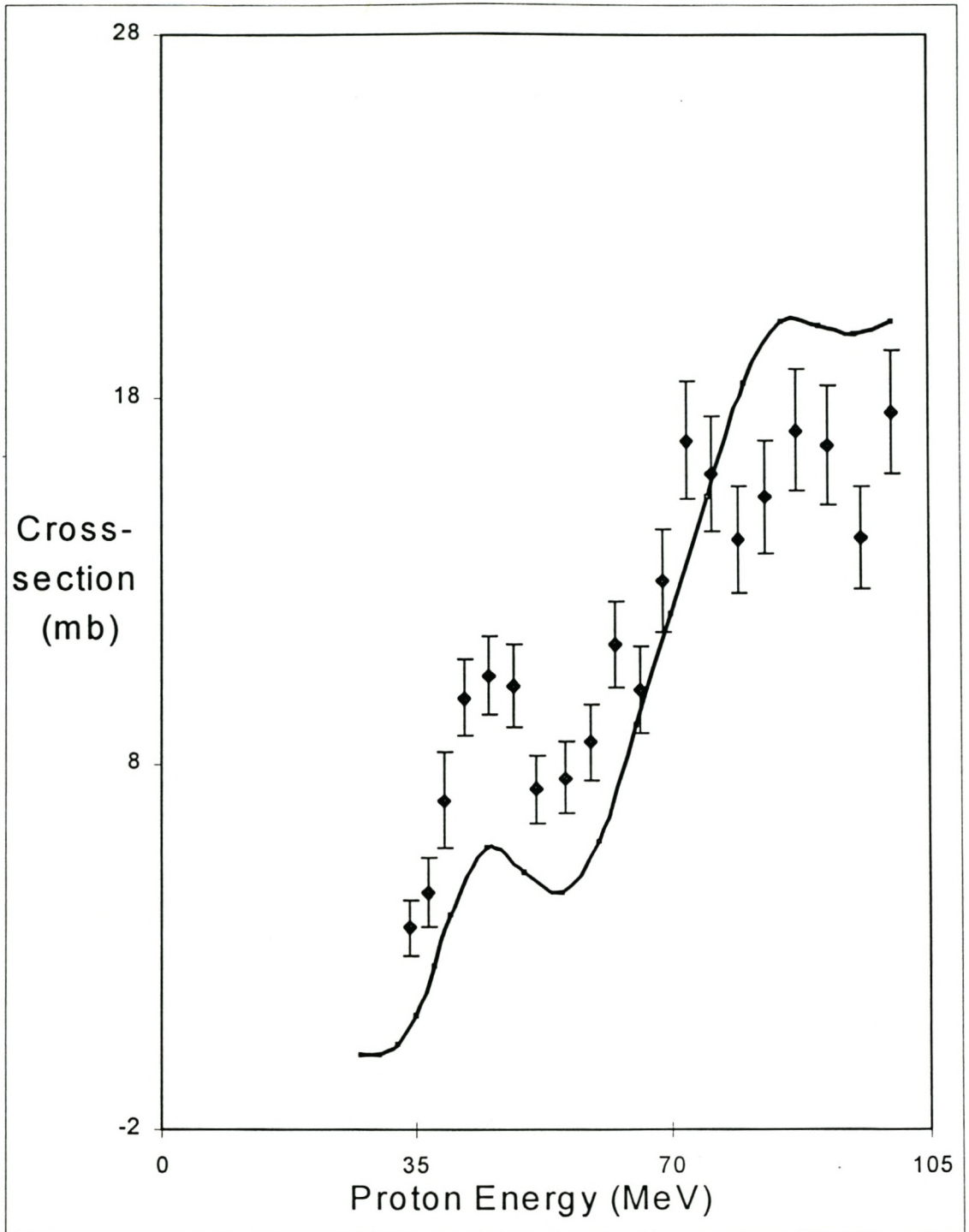


Figure 4-14: Experimental excitation functions for the production of ^{74}As in the bombardment of ^{nat}Br with protons and the theoretical calculations of Alice (solid line).

Chapter 5

Conclusion

In this chapter the important aspects of the production of ^{75}Se are reviewed and suggestions are made for future work in this area.

5.1 Conclusion

Normally ^{75}Se is produced in reactors via the $^{74}\text{Se}(n,\gamma)^{75}\text{Se}$ reaction. Accelerator production of carrier-free ^{75}Se via (p,n) reactions on ^{75}As has been suggested by Mushtaq et al. [Mus89]. In this study an alternative and new production route via proton bombardment of ^{nat}Br is explored. Excitation functions for $^{nat}\text{Br} + p$ were measured up to 100 MeV by means of the stacked-foil technique with the emphasis on the production of ^{75}Se . In order to develop a production route it is essential to have accurate excitation function data available. As seen from the literature survey done (refer to § 1.3), no existing data sets for this route could be found. The measurements in this study therefore not only enable the NAC to develop an optimum production route for ^{75}Se , but also make an important contribution to the expansion of the existing cross section data base found in the literature.

The experimental work resulted in the measurement of 11 excitation functions, which included selenium, bromine, krypton and arsenic radioisotopes. The selenium and arsenic isotopes are presented as new sets of data, while the data sets of bromine and krypton are compared with previously published data. In general the agreement between the new and existing cross

section data appears to be satisfactory and discrepancies were found in only a few cases. The values obtained from the theoretical calculations done with the computer code ALICE (IPPE) agreed within a factor of two with the experimental measurements. The shapes of the excitation functions are also very well represented by ALICE (IPPE).

A thick target yield calculation based on the experimental excitation function of ^{75}Se was done to obtain the incident energy which will result in the maximum yield for routine production at the NAC with its 66 MeV proton beam. At the end of bombardment the observed selenium radiocontaminants, ^{72}Se and ^{73}Se , predominate over the ^{75}Se . However, comparing the 119.8 days [Reu83] half-life of ^{75}Se to the 8.40 days [Reu83] of ^{72}Se and the 7.15 hours [Reu83] of ^{73}Se , it is still possible to produce a pure ^{75}Se containing less than 1% ^{72}Se by performing the chemical separation 72 days after the end of bombardment. After this period a production rate of 0.0280 mCi/ μAh is expected, which is more than twice the experimental yield of the commonly used $^{75}\text{As}(p,n)$ process.

Therefore, it appears that this new production route of ^{75}Se via proton bombardment of ^{nat}Br is superior to other existing accelerator routes.

It is suggested that proper thick target yield measurements be done to confirm the calculated values presented in § 4-2. As it is possible to generate a 200 MeV proton beam, the cross section measurements can be expanded for the 100 - 200 MeV energy range. In the case where ^{75}Se is routinely produced it is suggested that the use of a tandem target is explored to increase the obtained yield value by using two energy windows e.g. 51.7 - 16.1 MeV and 65.7 - 55.5 MeV.

Appendix A

The Calculation of the Stopping Power of a Charged Particle in the Target Material.

The computer programmes FOIL, STACK and STOPPING were used to calculate the energy loss in the foil stacks. The expressions used in these programmes are from Andersen and Ziegler [And77]. The stopping power values are given in units of MeV/(g.cm⁻²).

A.1 The high energy region

For particle energies above 1 MeV/nucleon, the stopping power is well described by the Bethe formula [Fan63]:

$$S(E) = \frac{4\pi e^4 Z_1^2 Z_2^2 B(v, Z_2)}{mv^2} \quad (\text{A1})$$

with

$$B(v, Z_2) = \ln \left[\frac{2mv^2}{I} \right] - \ln \left[1 - \frac{v^2}{c^2} \right] - \frac{v^2}{c^2} - \frac{C}{Z_2}, \quad (\text{A2})$$

where e is the electron charge, m the electron mass, Z_1 the atomic number of the charged particle, Z_2 the atomic number of the target, v the velocity of the charged particle, c the

velocity of light, I the mean ionisation potential and $\frac{C}{Z_2}$ the shell correction term.

Andersen and Ziegler used equations A1 and A2 as a model to fit experimental stopping powers. The authors then presented the following expression [And77] for the calculation of the stopping powers in the high-energy region:

$$S(E) = \frac{G_6}{\left(\frac{v^2}{c^2}\right)} \left[\ln \left(\frac{G_7 \frac{v^2}{c^2}}{1 - \frac{v^2}{c^2}} \right) - \frac{v^2}{c^2} - \sum_{i=0}^4 G_{8+i} (\ln E)^i \right]. \quad (\text{A3})$$

In this equation, and those to follow, G_j is a fitting parameter.

A.2 The low-energy region

In the energy region below 10 keV/nucleon the stopping power is proportional to the particle velocity, so that the fitting function is given by [And77]

$$S(E) = G_1 E^{0.5}. \quad (\text{A4})$$

A.3 The intermediate energy region

In the energy region, 10 keV/nucleon - 1 MeV/nucleon, no theory exists. Andersen and Ziegler used interpolation [And77] to fit the existing data by the use of

$$\frac{1}{S(E)} = \frac{1}{S_{low}} + \frac{1}{S_{high}} \quad (\text{A5})$$

where

$$S_{low} = G_2 E^{0.45} \quad (\text{A6})$$

and

$$S_{high} = \left(\frac{G_3}{E} \right) \ln \left[1 + \left(\frac{G_4}{E} \right) + (G_5 E) \right]. \quad (\text{A7})$$

A.4 Calculation of energy loss

The target material is divided into a large number, n , of thin slabs of thickness dx . The energy loss dE_i in the i th slab is then calculated by means of the expression

$$dE_i = fS_i dx \quad \text{for } 1 \leq i \leq n, \quad (\text{A8})$$

where f is a conversion factor depending on the units used and S_i the average stopping power in the particular slab.

To calculate S_i , the average energy

$$\langle E_i \rangle \approx E_i - \frac{dE_i}{2} \quad (\text{A9})$$

(with E_i the incident energy relevant to slab i) is used in

$$S_i = S(\langle E_i \rangle). \quad (\text{A10})$$

This energy loss process is repeated for all the specified slabs or until the particle is stopped in one of the slabs.

A.5 Stopping power in compounds and mixtures

The stopping power (S_{compound}) of a compound $A_x B_y$ is calculated by adding the weighted stopping power values for the components according to the additivity (Bragg's) rule [Jan82]:

$$S_{\text{compound}} = xS_A + yS_B \quad (\text{A11})$$

with

$$x + y = 1. \quad (\text{A12})$$

Appendix B

Calculation of cross sections and yields from stacked-foil data.

B.1 The relation between cross section and decay rate

The determination of reaction cross sections from stacked-foil experiments is based on two important relations. The first is the rate (R_{nucl}) at which a particular radioisotope is produced when a proton beam hits a target foil [Hel83]:

$$R_{nucl} = \frac{dN}{dt} = N_0 I \sigma, \quad (\text{B1})$$

with N the number of nuclei of the radioisotope, N_0 the number of target atoms per square cm in the foil, I the number of protons per second incident on the foil and σ the cross section for the production of the radioisotope.

Here N_0 is given by

$$N_0 = \frac{\Delta x N_A}{A}, \quad (\text{B2})$$

where N_A is Avogadro's number (mole^{-1}), A is the atomic mass of the foil material (g/mole) and Δx is the foil thickness (g/cm^2).

The other relation is the decay rate of the radioisotope, A_D , given by [Hel83]:

$$A_D = -\frac{dN}{dt} = N\lambda \quad (\text{B3})$$

with λ the radioisotope's decay constant (equal to $\frac{\ln 2}{T_{1/2}}$ and $T_{1/2}$ its half-life).

B.2 Activity build-up during bombardment

For the following formulae time points are defined as:

- $t_0 = 0$ is the start of the bombardment,
 - t_1 is the end of bombardment (EOB),
 - t_2 is the start of the counting period and
 - t_3 is the end of the counting period,
- with $t_0 < t_1 < t_2 < t_3$.

The activity $dA_D(t)$ produced in a small time interval dt at a time t during bombardment follows from equations (B1) and (B2) as

$$dA_D(t) = \lambda R_{nucl} dt. \quad (\text{B4})$$

At EOB this activity will have decayed to the value $dA_D(t_1)$ given by

$$\begin{aligned} dA_D(t_1) &= \lambda R_{nucl} dt \exp[-\lambda(t_1 - t)], \\ 0 &\leq t \leq t_1. \end{aligned} \quad (\text{B5})$$

Integrating equation (B5) gives the total activity $A_D(t_1)$ produced at EOB:

$$A_D(t_1) = R_{nucl}[1 - \exp(-\lambda t_1)]. \quad (\text{B6})$$

B.3 Activity after bombardment

After the bombardment the induced activity of the radioisotope follows the normal decay law according to the expression [Hel83]

$$\begin{aligned} A_D(t) &= A_D(t_1) \exp[-\lambda(t - t_1)], \\ t_1 &\leq t \leq t_2. \end{aligned} \quad (\text{B7})$$

B.4 Decay during counting

Sometimes in the measuring of a radioisotope's activity its half-life is comparable to the duration of the counting time. In such circumstances only a "mean" activity can be determined, due to the noticeable activity change during the counting time. The total disintegrations dN occurring in a small time dt , at time t during counting, can then be written as

$$dN = A_D(t_2) \exp[-\lambda(t - t_2)]dt \quad (\text{B8})$$

where $t_2 < t < t_3$.

By integrating the above-mentioned equation the total number of disintegrations N during the counting time $(t_3 - t_2)$ is given by

$$N = \int dN = A_D(t_2) \int_{t_2}^{t_3} \exp[-\lambda(t - t_2)]dt. \quad (\text{B9})$$

The "mean" activity during the counting then follows as

$$\frac{N}{t_3 - t_2} = \frac{A_D(t_2)}{t_3 - t_2} \int_{t_2}^{t_3} \exp[-\lambda(t - t_2)] dt. \quad (\text{B10})$$

It is necessary to compensate for decay during counting. For this the point in time, t_m , where the actual activity value is equal to the measured “mean” activity, has to be obtained; therefore

$$A_D(t_m) = A_D(t_2) \exp[-\lambda(t_m - t_2)] = \frac{N}{t_3 - t_2}. \quad (\text{B11})$$

By using (B10) and (B11) it follows that

$$t_m = t_2 + \frac{1}{\lambda} \ln \left[\frac{\exp[-\lambda(t_3 - t_2)] - 1}{\lambda(t_3 - t_2)} \right]. \quad (\text{B12})$$

B.5 Reaction cross sections

For the following derivations, the following experimentally measured time intervals are defined:

bombardment time	$t_b = t_1 - t_0 = t_1$
decay time	$t_d = t_2 - t_1$ and
counting time	$t_c = t_3 - t_2$.

A radioisotope’s activity in a specific foil is determined from the total counts in a characteristic peak, A_p , in its gamma-ray spectrum. The “mean” activity $A_D(t_m)$ is then calculated using

$$A_D(t_m) = \frac{A_p}{t_c \epsilon_E \epsilon_\gamma}, \quad (\text{B13})$$

with ϵ_E the detector efficiency value for the gamma-ray of energy E , and ϵ_γ the branching ratio of that gamma-ray.

The expression for the calculation of the cross section (σ) can then be obtained using equations (B12), (B11), (B7), (B6), (B1) and (B13):

$$\sigma(cm^2) = \frac{A_p t_b}{t_c \epsilon_E \epsilon_\gamma I_t N_0 [1 - \exp(-\lambda t_b) \exp[-\lambda(t_m - t_b)]]}. \quad (B14)$$

Here, I_t is the total number of protons incident on the target foil. This is given by

$$I_t = I t_b = K_1 C_t, \quad (B15)$$

with $C_t(\mu Ah)$ the integrated charge and $K_1 = 2.24692 \times 10^{16}$ is the number of protons per μAh .

B.6 Thin target yield

The thin target yield (production rate of a radioisotope) is measured in terms of activity per unit charge (integrated beam current) and expressed in the unit of Ci/ $(\mu Ah \cdot MeV)$. Using equations (B1), (B2), (B3) and (B15) the yield in a thin foil is defined as

$$R_{diff}(\text{Ci}/(\mu Ah \cdot MeV)) = \frac{R_{nucl}}{I \Delta E} = \frac{\lambda K_1 N_A \sigma}{AS(E_{av})}, \quad (B16)$$

where the proton energy loss in the foil is given by

$$\Delta E = S(E_{av}) \Delta x \quad (B17)$$

with $S(E_{av})$ the stopping power for protons of energy E_{av} in the target. Here E_{av} indicates the average energy,

$$E_{av} = \frac{E_{in} + E_{out}}{2}, \quad (B18)$$

in the foil.

B.7 Thick target yield

Thin target yield is a function of proton energy. By integrating equation (B16) over the energy range used, the rate R_{thick} at which a particular radioisotope is produced in a thick target is

then given by the expression

$$R_{thick}(E_{in}) = \int_0^{E_{in}} R_{diff}(E)dE, \quad (B19)$$

with E_{in} the incident proton energy.

B.8 Analysis programs

These formulae were taken from the computer program, SIGMA and incorporated into a *Microsoft Excel* spreadsheet to calculate the cross sections and thin target yields for the different radioisotopes. Thick target yields were calculated by the use of the program YIELD.

Appendix C

Measured cross sections for the Radioisotopes Produced in the Monitor Foils.

Table C.1 *Measured cross section values for the production of ^{62}Zn in the bombardment of ^{nat}Cu with 40 MeV protons, before and after adjustments.*

Before Adjustments		After Adjustments	
Proton Energy (MeV)	cross section (mb)	Proton Energy (MeV)	cross section (mb)
37.6	14.3 ± 1.2	36.0	13.3 ± 1.2
35.2	17.8 ± 1.5	33.8	16.6 ± 1.4
32.5	24.2 ± 2.1	31.4	22.6 ± 1.9
29.8	38.7 ± 3.2	28.8	36.1 ± 3.0
26.8	63.0 ± 5.2	25.9	58.8 ± 4.8
23.5	70.3 ± 5.7	22.7	65.6 ± 5.4
21.1	59.1 ± 4.8	20.2	55.2 ± 4.6
18.5	38.5 ± 3.2	17.5	35.9 ± 2.9
15.6	8.35 ± 0.70	14.4	7.80 ± 0.66

The adjustments to the proton energies were done using the relation

$$E_{p'} = E_p + \Delta y, \quad (\text{C1})$$

with E_p the proton energy (MeV) before adjustment and Δy (MeV) the value of the fitting function:

$$\Delta y = 1.06 - 1.07 \exp(-17513217 E_p^{-5.33}), \quad (\text{C2})$$

as discussed in § 3.2.6.4.

Table C.2 Measured cross section values for the production of ^{22}Na in the bombardment of ^{nat}Al with 66 MeV protons, before and after adjustments.

Before Adjustments		After Adjustments	
Proton Energy (MeV)	Cross section (mb)	Proton Energy (MeV)	Cross section (mb)
64.7	22.5 ± 1.8	64.8	23.8 ± 1.9
61.0	24.2 ± 2.0	61.5	25.5 ± 2.1
57.2	26.9 ± 2.2	58.1	28.4 ± 2.3
53.2	31.0 ± 2.5	54.5	32.8 ± 2.7
48.9	35.1 ± 2.9	50.6	37.1 ± 3.0
45.5	39.6 ± 3.2	47.5	41.9 ± 3.4
41.8	41.2 ± 3.4	44.1	43.5 ± 3.5
37.8	38.2 ± 3.1	40.4	40.3 ± 3.3
34.8	30.1 ± 2.5	37.6	31.7 ± 2.6
31.6	16.4 ± 1.3	34.6	17.4 ± 1.4
28.0	4.35 ± 0.36	31.3	4.60 ± 0.38
24.1	0.364 ± 0.031	27.6	0.384 ± 0.032

The adjustments to the proton energies were done using equation (C1) with a fitting function value of

$$\Delta y = 4.66 - 0.0332E_p - 0.000571(E_p)^2, \quad (\text{C3})$$

with E_p the proton energy (MeV) before adjustment.

Table C.3 Summary of the measured cross section values for the production of ^{22}Na in the bombardment of ^{nat}Al with 100 and 66 MeV protons.

Proton Energy (MeV)	Cross section (mb)	Proton Energy (MeV)	Cross section (mb)
99.3	18.8 ± 1.5	54.5	32.8 ± 2.7
94.9	18.6 ± 1.5	50.6	37.1 ± 3.0
90.4	19.4 ± 1.6	47.5	41.9 ± 3.4
86.3	19.6 ± 1.6	44.1	43.5 ± 3.5
82.1	20.1 ± 1.6	40.4	40.3 ± 3.3
78.4	20.4 ± 1.7	38.3	33.2 ± 2.7
74.6	20.3 ± 1.7	37.6	31.7 ± 2.6
71.3	21.3 ± 1.8	35.8	23.2 ± 1.9
67.9	22.5 ± 1.9	34.6	17.4 ± 1.4
64.8	23.8 ± 1.9	33.3	11.3 ± 0.92
64.5	23.8 ± 2.0	31.3	4.60 ± 0.38
61.5	25.5 ± 2.1	30.5	2.51 ± 0.21
60.9	25.9 ± 2.2	27.6	0.384 ± 0.032
58.1	28.4 ± 2.3	24.4	0.00962 ± 0.00917
57.1	29.4 ± 2.4		

Appendix D

Measured cross sections for the Radioisotopes Produced in Br.

Table D1: *Measured cross section values for the production of ^{74}As and ^{71}As*

Proton Energy (MeV)	cross section (mb)		Proton Energy (MeV)	cross section (mb)
	^{74}As	^{71}As		^{74}As
100	17.6 ± 1.7	14.5 ± 1.2	62.5	11.2 ± 1.2
95.7	14.2 ± 1.4	15.0 ± 1.2	59.1	8.61 ± 1.0
91.2	16.7 ± 1.6	15.2 ± 1.2	55.5	7.61 ± 0.98
87.1	17.1 ± 1.6	14.8 ± 1.2	51.7	8.31 ± 0.94
82.9	15.3 ± 1.5	13.7 ± 1.1	48.6	10.1 ± 1.1
79.2	14.1 ± 1.5	10.9 ± 0.90	45.3	10.4 ± 1.1
75.4	15.9 ± 1.6	7.34 ± 0.64	41.8	9.82 ± 1.0
72.2	16.8 ± 1.6	4.65 ± 0.39	39.2	7.01 ± 1.3
68.9	13.0 ± 1.4	2.01 ± 0.21	36.8	4.46 ± 0.97
65.7	10.0 ± 1.2	0.919 ± 0.17	34.2	3.49 ± 0.76

Table D.2: Measured cross section values for the production of ^{80m}Br , ^{77}Br and ^{75}Br

Proton Energy (MeV)	cross section (mb)		
	^{80m}Br	^{77}Br	^{75}Br
100	19.5 ± 1.6	111 ± 11	37.4 ± 3.0
95.7	20.6 ± 1.7	116 ± 11	38.1 ± 3.1
91.2	21.7 ± 1.8	119 ± 11	39.3 ± 3.2
87.1	23.0 ± 1.9	135 ± 13	39.0 ± 3.2
82.9	24.2 ± 2.0	139 ± 13	40.6 ± 3.3
79.2	25.1 ± 2.0	148 ± 14	41.7 ± 3.4
75.4	25.8 ± 2.1	158 ± 14	44.8 ± 3.7
72.2	26.1 ± 2.1	168 ± 15	47.0 ± 3.8
68.9	26.6 ± 2.2	170 ± 15	50.4 ± 4.1
65.7	25.9 ± 2.1	178 ± 16	44.8 ± 0.24
62.5	26.5 ± 2.1	189 ± 17	41.3 ± 0.21
59.1	27.1 ± 2.2	176 ± 16	30.5 ± 0.15
55.5	28.4 ± 2.3	163 ± 15	15.6 ± 0.073
51.7	29.4 ± 2.4	149 ± 14	5.52 ± 0.025
48.6	31.0 ± 2.5	166 ± 15	1.78 ± 0.010
45.3	32.2 ± 2.6	210 ± 18	0.577 ± 0.0031
41.8	33.2 ± 2.7	244 ± 21	0.321 ± 0.0022
39.2	43.3 ± 3.5	247 ± 24	-
36.8	41.8 ± 3.4	267 ± 25	-
34.2	42.0 ± 3.4	245 ± 21	-
31.5	48.2 ± 3.9	221 ± 20	-
28.5	54.2 ± 4.4	139 ± 13	-
25.3	53.8 ± 4.4	38.6 ± 4.9	-
21.6	38.2 ± 3.1	-	-
18.9	25.0 ± 2.0	-	-
16.1	8.49 ± 0.69	-	-
12.9	0.813 ± 0.070	-	-

Table D.3: Measured cross section values for the production of ^{79}Kr , ^{77}Kr and ^{76}Kr

Proton Energy (MeV)	cross section (mb)		
	^{79}Kr	^{77}Kr	^{76}Kr
100	17.1 ± 1.5	15.8 ± 1.3	5.63 ± 0.79
95.7	20.4 ± 1.8	17.6 ± 1.4	5.06 ± 0.66
91.2	20.0 ± 1.8	19.2 ± 1.6	7.05 ± 0.90
87.1	22.7 ± 1.9	20.8 ± 1.7	7.01 ± 0.64
82.9	24.8 ± 2.2	23.3 ± 1.9	7.84 ± 0.71
79.2	26.0 ± 2.3	26.7 ± 2.2	7.88 ± 0.72
75.4	29.6 ± 2.6	30.4 ± 2.5	9.05 ± 0.82
72.2	30.0 ± 2.6	33.9 ± 2.8	8.91 ± 0.81
68.9	32.3 ± 2.7	38.1 ± 3.1	8.59 ± 0.78
65.7	34.7 ± 2.9	37.8 ± 3.1	9.38 ± 0.84
62.5	39.2 ± 3.3	41.7 ± 3.4	10.6 ± 0.93
59.1	42.1 ± 3.5	40.6 ± 3.3	13.8 ± 1.2
55.5	46.9 ± 3.9	35.4 ± 2.9	16.1 ± 1.4
51.7	47.5 ± 3.9	27.9 ± 2.3	15.7 ± 1.3
48.6	62.0 ± 5.1	35.8 ± 2.9	14.9 ± 1.3
45.3	87.5 ± 7.2	53.6 ± 4.3	12.6 ± 1.1
41.8	120 ± 9.8	72.1 ± 5.9	8.09 ± 0.71
39.2	170 ± 14	119 ± 9.6	3.76 ± 0.77
36.8	197 ± 16	122 ± 9.9	86.9 ± 7.2
34.2	228 ± 18	117 ± 9.5	86.7 ± 7.2
31.5	236 ± 19	102 ± 8.2	75.6 ± 6.1
28.5	202 ± 16	55.8 ± 4.5	69.2 ± 5.6
25.3	118 ± 9.6	7.33 ± 0.60	50.7 ± 4.1
21.6	27.0 ± 2.2	-	34.2 ± 2.8
18.9	35.2 ± 2.9	-	23.9 ± 1.9
16.1	81.7 ± 6.6	-	15.3 ± 1.2
12.9	244 ± 20	-	21.5 ± 1.7

Table D.4: Measured cross section values for the production of ^{75}Se , ^{73}Se and ^{72}Se

Proton Energy (MeV)	cross section (mb)		
	^{75}Se	^{73}Se	^{72}Se
100	108 ± 9.1	24.4 ± 2.0	7.17 ± 0.75
95.7	106 ± 8.9	22.4 ± 1.8	6.82 ± 0.73
91.2	109 ± 9.2	21.4 ± 1.7	5.94 ± 0.65
87.1	104 ± 8.7	18.6 ± 1.5	5.63 ± 0.64
82.9	101 ± 8.5	16.1 ± 1.3	4.49 ± 0.56
79.2	108 ± 9.1	13.7 ± 1.1	4.97 ± 0.57
75.4	108 ± 8.9	11.7 ± 0.96	6.50 ± 0.63
72.2	111 ± 9.3	10.4 ± 0.85	7.35 ± 0.70
68.9	117 ± 9.7	10.4 ± 0.86	7.41 ± 0.70
65.7	115 ± 9.3	11.1 ± 0.90	6.19 ± 0.51
62.5	104 ± 8.4	13.4 ± 1.1	4.42 ± 0.36
59.1	86.5 ± 7.0	16.9 ± 1.4	2.42 ± 0.20
55.5	60.0 ± 4.9	18.0 ± 1.5	0.677 ± 0.062
51.7	41.7 ± 3.4	15.8 ± 1.3	0.107 ± 0.016
48.6	29.5 ± 2.4	11.7 ± 0.96	-
45.3	19.8 ± 1.6	5.32 ± 0.44	-
41.8	13.2 ± 1.1	1.57 ± 0.14	-
39.2	7.60 ± 1.8	-	-
36.6	9.80 ± 1.7	-	-
34.2	18.0 ± 2.3	-	-
31.5	23.5 ± 2.5	-	-
28.5	27.8 ± 2.8	-	-
25.3	28.9 ± 2.9	-	-
21.6	20.7 ± 2.3	-	-
18.9	11.8 ± 1.6	-	-
16.1	2.50 ± 0.69	-	-

Appendix E

Input parameters used in calculations with the computer code **ALICE (IPPE)**

In ALICE (IPPE) the geometry dependent hybrid (GDH) model is used for preequilibrium nuclear emission. The equilibrium decay of the residual compound nucleus was treated by using the Weiskopf-Ewing formalism where all four types of particle evaporation (neutron, proton, alpha and deuteron) were considered. The following set of input parameters was used:

AP = 1.0	Projectile mass number
AT = 79.0 or 81.0	Target mass number
ZP = 1.0	Projectile atomic number
ZT = 35.0	Target atomic number
ED = 0.20	An energy bin size of 0.20 MeV was specified.
INVER = 0	The optical model is used to calculate the inverse cross sections.
JCAL = 1	The Weiskopf-Ewing evaporation theory is used for the equilibrium calculation.
M3 = 4	The number and type of particles to be emitted from each nuclide; in this case protons, neutrons, deuterons and alpha particles.

MC = 10	Where available the calculated mass values of Myers and Swiatecki were substituted by the experimental mass values of the 1983 Wapstra-Audi mass table.
MP = 3	Normal pairing shift
LDOPT = 2	Ignatyuk (IPPE) level densities
PLD = 9.0	Level density parameter = ACN / 9.0
CLD = 1.0	The ratio of nucleon to fission level density parameters
IFIS = 0	The rotating finite range barriers of A.J. Sierk are used.
BARFAC = 1.0	Multiplier of fission barrier

Default values were used for the other parameters.

Bibliography

- [And77] Andersen H.H. and Ziegler J.F. Hydrogen stopping powers and ranges in all elements. In *Stopping and Ranges of Ions in Matter* (Ed. Ziegler J.F.), Vol 3, p. 1. Pergamon, New York (1977).
- [Ble94] Blessing G., Lavi N., Hashimoto K., Qaim S.M. Thermochematographic separation of Radioselenium from Irradiated Cu₃As-target: Production of no-carrier added ⁷⁵Se. *Radiochim. Acta.* **65**, 93 (1994).
- [Blo55] Blosser H.G., Handley T.H., Survey of (p,n) reactions at 12 MeV. *Phys. Rev* **100**, 1340 (1955).
- [Bod93] Bodeman R. et al. Production of residual nuclei by proton-induced reactions on C, N, O, Mg, Al and Si. *Nucl. Instr. Meth. B.* **82**, 9 (1993).
- [Bro86] Browne E. and Firestone R.B. *Table of Radioactive Isotopes* (Ed. Shirley V.S.). John Wiley & Sons, New York (1986).
- [Col74] Colle R., Kishore R. Excitation Functions for (p,n) Reactions on ⁷⁹Br and ¹²⁷I. *Phys. Rev. C* **9**, 2166 (1974).
- [Dej79] De Jongh D., Brinkman G.A., Linder L. Excitation Functions for the production of ⁷⁶Kr and ⁷⁷Kr. *Int.J.Appl.Radiat.Isot.* **30**, 188 (1979).
- [Dhi96] Dhillion K., Dhillion S.K. Isotopes and Radiations in Agriculture and Enviroment Research, New Deli (India). In *Indian Society for Nuclear Techniques in Agriculture and Biology.* **336**, 112 (Oct 1996).

- [Dik79] Diksic M, Galinier J.L., Marshall H., Yaffe L. ^{79}Br and ^{81}Br (p,xn) and (p,pxn) Excitation Functions in the Energy Range 10-85 MeV. *Phys. Rev. C* **19**, 1753 (1979).
- [Eng90] Engelskirchen G., Hamacher K., Stocklin G. Basic studies on a selenation strategy via triphenylphosphineselenide using non-carrier added selenium-75. In *International Symposium on Radiopharmaceutical Chemistry*, John Wiley & Sons, New York (1990).
- [Enz82] Enzmann P.J. In-vivo labelling of viral proteins with ^{75}Se selenomethionine. *J. Virolog. Meth.* **5**, 243 (1982).
- [Fan63] Fano U. Penetration of protons, alpha particles, and mesons. *Ann. Rev. Nucl. Sci.* **13**, 1 (1963).
- [Fas98] Fassbender M., NAC, Faure, South Africa (1998) (*private communication*).
- [Hat72] Hatchette J.B. et al. Scintiphotos of the pancreas: Analysis of 134 studies. *J. Nucl. Med.* **13**, 51 (1972).
- [Hel83] Helus F. and Wolber G. In *Radionuclides Production* (Ed. Helus F.). Vol **1**, p.57, CRC Press Inc., Florida, U.S.A. (1983).
- [Jan82] Janni J.F. (1982) Proton range-energy table, 1 keV - 10 GeV. *At. Nucl. Data Tables* **27**, 150 (1982).
- [Kno79] Knoll G. F. In *Radiation detection and measurement*. John Wiley & Sons, New York (1979).
- [Kra88] Krane K. In *Introductory Nuclear Physics*. John Wiley & Sons, New York (1988).
- [Mil92] Mills S.J., Steyn G.F., Nortier F.M. Experimental and theoretical excitation functions of radionuclides produced in proton bombardment of copper up to 200 MeV. *Int. J. Appl. Radiat. Isot.* **43**, 1019 (1992).
- [Mus89] Mushtaq A., Qaim S.M., Stöcklin G. Production of ^{73}Se via (p,3n) and (d,4n) Reactions on Arsenic. *Int. J. Appl. Radiat. Isot.* **39**, 1085 (1988).
- [Nor90] Nortier F.M., Ph.D Thesis. University of Stellenbosch, Stellenbosch, South Africa (1990) (unpublished).

- [Ple90] Plenevaux A., Guillaume M., Brihaye C., Lemaire C., Cantineau R. Chemical processing for production of no-carrier added selenium-73 from germanium and arsenic targets and synthesis of L-2-Amino-4-([⁷³Se]Methylseleno) butyric acid (L-[⁷³Se]Selenomethionine). *Appl. Radiat. Isot.*, **41**, 829 (1990).
- [Qai82] Qaim S.M. Nuclear data relevant to cyclotron produced short-live medical radioisotopes. *Radiochim. Acta* **30**, 147 (1982).
- [Qai88] Qaim S.M. Medical isotopes and nuclear data. In *Proceedings of the IAEA consultants' meeting on data requirements for medical radioisotope production*. p.25 (January 1998).
- [Qai90] Qaim S.M. Nuclear Data for Medical Radioisotope Production using charged particles of Energy above 20 MeV. In *Proceedings of the advisory group meeting for intermediate energy nuclear data for applications, Vienna*. p.45 (October 1990).
- [Reu83] Reus U. and Westmeier W. Catalog of Gamma Rays from Radioactive Decay. *At. Nucl Data Tables*, **29**, Parts 1 and 2 (1983).
- [Ste90a] Steyn G.F., Mills S.J., Nortier F.M., Simpson B.R.S., Meyer B.R. Production of ⁵²Fe via Proton-induced Reactions on Manganese and Nickel. *Int.J.Appl.Radiat.Isot.* **41**, 315 (1990).
- [Ste90b] Steyn G.F., Ph.D Thesis. University of Stellenbosch, Stellenbosch, South Africa (1990) (unpublished).
- [Wee86] Weeks K.J. and Schulz R.J. Selenium-75: A potential source for use in high-activity brachytherapy irradiators *Med. Phys.* **13**(5) Sep/Oct 1986.
- [Zai91] Zaitseva, N.G., Deptula C., Knotek O., Khan K.S., Mikolaewski S., Mikec P., Rurarz E., Khalkin V.A., Konov V.A., Popinenkova L.M. cross sections for the 100 MeV Proton-induced Nuclear Reactions and Yields of some Radionuclides used in Nuclear Medicine. *Radiochim. Acta* **54**, 57 (1991).